AWARD NUMBER:
W81XWH-13-1-0043

TITLE:
Defining the Role of Autophagy Kinase ULK1 Signaling in Therapeutic Response of Tuberous Sclerosis Complex to mTOR Inhibitors

PRINCIPAL INVESTIGATOR:
Reuben J. Shaw, Ph.D.

CONTRACTING ORGANIZATION:
The Salk Institute for Biological Studies
La Jolla, CA 92037

REPORT DATE:
July 2016

TYPE OF REPORT:
Final Report

PREPARED FOR: U.S. Army Medical Research and Materiel Command
Fort Detrick, Maryland 21702-5012

REPORT DOCUMENTATION PAGE

Form Approved
OMB No. 0704-0188

1. REPORT DATE	2. REPORT TYPE	3. DATES COVERED
July 2016	Final	1 Apr 2013 - 31 Mar 2016

4. TITLE AND SUBTITLE

Defining the Role of Autophagy Kinase ULK1 Signaling in Therapeutic Response of Tuberous Sclerosis Complex to mTOR Inhibitors

5a. CONTRACT NUMBER

5b. GRANT NUMBER
W81XWH-13-1-0043

5c. PROGRAM ELEMENT NUMBER

6. AUTHOR(S)
Shaw, Reuben J.

E-Mail: shaw@salk.edu

5d. PROJECT NUMBER

5e. TASK NUMBER

5f. WORK UNIT NUMBER

7. PERFORMING ORGANIZATION NAME(S) AND ADDRESS(ES) AND ADDRESS(ES)

The Salk Institute for Biological Studies
10010 North Torrey Pines Road
La Jolla, CA 92037-1002

8. PERFORMING ORGANIZATION REPORT NUMBER

9. SPONSORING / MONITORING AGENCY NAME(S) AND ADDRESS(ES)

U.S. Army Medical Research and Materiel Command
Fort Detrick, Maryland 21702-5012

10. SPONSOR/MONITOR'S ACRONYM(S)

11. SPONSOR/MONITOR'S REPORT NUMBER(S)

12. DISTRIBUTION / AVAILABILITY STATEMENT

Approved for Public Release; Distribution Unlimited

13. SUPPLEMENTARY NOTES

14. ABSTRACT

The Tuberous Sclerosis Complex tumor suppressors are known to be critical negative regulators of the mTORC1 kinase complex that controls cell growth and autophagy. Our laboratory and others have recently decoded a major conserved route that mTORC1 uses to control autophagy. These studies demonstrate that mTORC1 inactivates another kinase complex composed of the autophagy kinase ULK1 and its associated subunits. One prediction of these findings is that in cells and tumors with TSC mutations and hyperactive mTOR, the ULK1 complex – and the process of autophagy – will be suppressed. There were two major aims for this funding period: 1) to further develop antibodies and reagents to readout ULK1-activity and substrate phosphorylation to see how well they act as biomarkers of mTOR inhibition, and 2) to further explore use of novel small molecule inhibitors of ULK1 to synergize with mTOR inhibitors to induce cell death.

15. SUBJECT TERMS
autophagy, cell survival, ULK1, phosphorylation, substrates, mTOR, rapamycin

16. SECURITY CLASSIFICATION OF:			17. LIMITATION OF ABSTRACT	18. NUMBER OF PAGES	19a. NAME OF RESPONSIBLE PERSON
a. REPORT	b. ABSTRACT	c. THIS PAGE			19b. TELEPHONE NUMBER *(include area code)*
Unclassified	Unclassified	Unclassified	Unclassified	52	USAMRMC

Standard Form 298 (Rev. 8-98)
Prescribed by ANSI Std. Z39.18

Table of Contents

Page

INTRODUCTION

The Tuberous Sclerosis Complex tumor suppressors are known to be critical negative regulators of the mTORC1 kinase complex that controls cell growth and autophagy. Our laboratory and others have recently decoded a major conserved route that mTORC1 uses to control autophagy. These studies demonstrate that mTORC1 inactivates another kinase complex composed of the autophagy kinase ULK1 and its associated subunits. One prediction of these findings is that in cells and tumors with TSC mutations and hyperactive mTOR, the ULK1 complex – and the process of autophagy – will be suppressed. There were two major aims for this funding period: 1) to further develop antibodies and reagents to readout ULK1-activity and substrate phosphorylation to see how well they act as biomarkers of mTOR inhibition, and 2) to further explore use of novel small molecule inhibitors of ULK1 to synergize with mTOR inhibitors to induce cell death.

BODY

Task 1: Examine how ULK1 activity and function in response to mTOR inhibitors

We determined that mTOR inhibitors, including rapamycin, and more potent small molecule catalytic mTOR inhibitors like INK128 (MLN-0128) and AZD8055, all result in loss of the mTOR-dependent phosphorylation of ULK1, and that this correlates with activation of ULK1 kinase activity. This data is seen in Figure 4, Figure 6, and Figure 7 of our Molecular Cell paper (*Egan et al., 2015* - attached in Appendix).

Task 2: Examination of our newly identified ULK1 substrates in TSC2-deficient cell types and tissues in response to mTOR inhibitors, including further mapping and identification of ULK1 phosphorylation sites in Vps34, Ambra1, and Beclin; development of phospho-specific antibodies and characterized response of these ULK1-dependent sites in response to mTOR inhibitors

We comprehensively mapped ULK1-dependent phosphorylation sites in Vps34, Ambra1, Beclin, Atg13, Atg101, Fip200 and report these findings in Figure 2 and Supplemental Figure 2 of *Egan et al, 2015*. These figures encompass the largest reporting of new ULK1-dependent phosphorylation sites to date in the scientific literature. Combined with the definition of the optimal ULK1 substrate motif and new assays we designed to assay ULK1 kinase activity in Figure 1 and Supplemental Figure 1 of that paper, it gives the field a toolbox and reference point for all future studies decoding events downstream of ULK1. Prior to our Egan et al paper, there was a single ULK1 substrate phosphorylation site known in mammalian cells, Atg13 Ser318 (reported in *Joo et al., 2011*). Since that time at least one additional ULK1 phosphorylation site has been mapped – Sec16A Ser846 (*Joo et al., 2016*), which matched perfectly to the consensus ULK1 substrate amino acid sequence we report in Figure 1 and 2 of *Egan et al., 2015*.

Task 4: Determine therapeutic response of TSC2+/-, ULK1-/- compound mutant mice vs. TSC2+/- mice to rapamycin and mTOR catalytic inhibitors

We ran into technical hurdles with accomplishing this task due to differing genetic backgrounds that the ULK1-/- mouse strain and TSC2+/- strain were on. We are still actively engaged in these mouse crosses and intend to publish the outcome of these studies at a future date.

Task 3: Define therapeutic response to mTOR inhibitors of xenografted TSC2-deficient MEFs and ELT3 tumor cells +/- ULK1 shRNA & Task 5: Pharmacological test of novel ULK1 kinase inhibitors in ability to regulate proliferation or survival in TSC-deficient cells when combined with mTOR inhibitors

In our *Egan et al. 2015*, Molecular Cell paper we report a highly selective ULK1 small molecular inhibitor, SBI-0206965, and devote Figure 4 and Supplemental Figure 4 to reporting the details of the screening we performed which led to hundreds of compound leads that after years of effort were narrowed to a single, effective agent SBI-0206965. We detail in Figure 5 and Supplemental Figure 5 of *Egan et al. 2015* the exquisite selectivity of SBI-0206965, which is more selective than multiple other similar small molecule ATP-competitive kinase inhibitors which are currently being used in the clinic for oncology purposes (see Figure S5B). We detail in Figure 6, Supplemental Figure 6, Figure 7, and Supplemental Figure 7, the use of this compound in multiple different tumor cell lines, both as single agent and in combination with three distinct mTOR inhibitors. We believe these results provide proof of principle data to encourage additional testing of this compound and derivatives of this compound in additional preclinical PDX and GEMM of Tuberous Sclerosis and multiple other cancer types.

Finally, we have recently made great headway on testing SBI-0206965 in ELT-3 cells, which was not included in the *Egan et al. 2015* paper. As seen in Figure 1 below, in ELT3 TSC-deficient tumor cells, we observe cell death induced in culture after treatment with SBI-0206965 as a single agent, which is further enhanced by dual treatment with the mTOR catalytic inhibitor AZD8055.

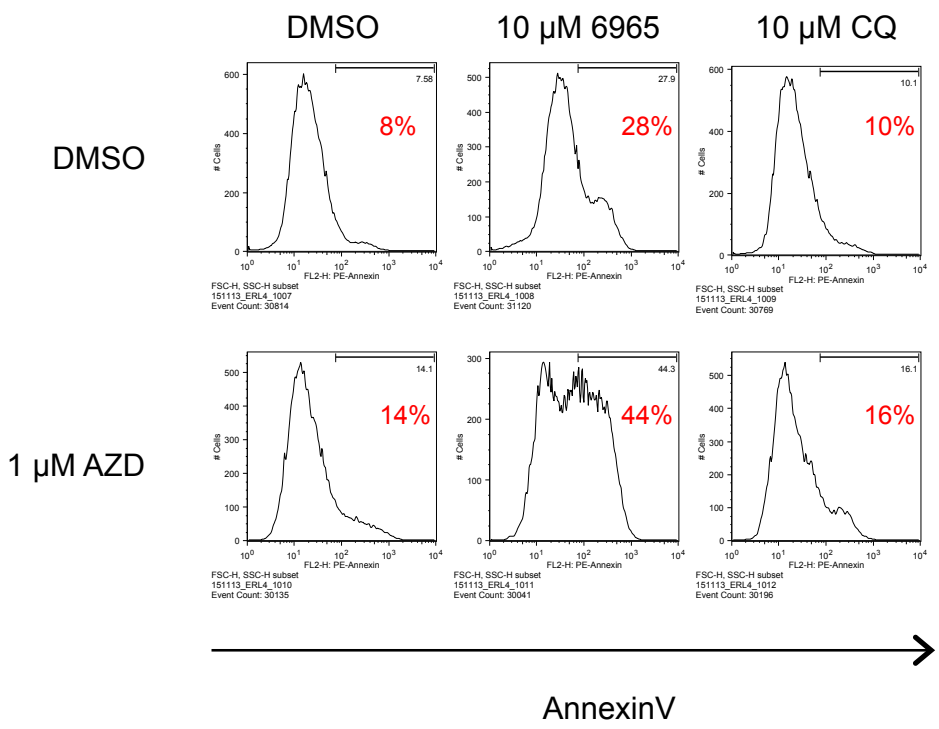

Figure 1. ULK1 inhibitor efficiently induces apoptosis in TSC-deficient ELT3 tumor cells as a single agent, which is enhanced by co-administration of a mTOR inhibitor *Treatment of ELT3 cells with 10uM of our novel ULK1 inhibitor compound SBI-0206965 ("6965") versus 10uM of the general autophagy inhibitor chloroquine ("CQ") with or without the catalytic mTOR inhibitor AZD-8055 ("AZD"). Cells were treated for 48 hours and then collected, stained with PE-AnnexinV and quantified by FACS analysis. Red numbers indicate the percentage of AnnexinV- positive cells, representing cells actively undergoing apoptosis.*

Future Work will be aimed at further testing the efficacy of SBI-0206965 in TSC-deficient cell lines and animal models to address whether this compound shows preclinical efficacy as a single agent, or in combination with rapamycin analogs for the treatment of various symptoms of Tuberous Sclerosis Complex.

KEY RESEARCH ACCOMPLISHMENTS:

- We discovered and reported that ULK1 directly phosphorylates multiple autophagy components, including VPS34 on Ser249
- We discovered SBI-0206965, the most selective ULK1 small molecular kinase inhibitor ever reported to date
- We demonstrated that SBI-0206965 combined with starvation or mTOR inhibition leads to ULK1 degradation which serves as a biomarker of drug efficacy in cell lines and in mouse tissues
- We demonstrated that SBI-0206965 synergizes with mTOR inhibition to induce cell death, providing a proof of concept to move further into pre-clinical models and ultimately into the clinic with this compound or derivatives of this compound

REPORTABLE OUTCOMES:

1. Importantly, we reported the outcomes of nearly all aspects of this grant in a single large all-encompassing paper in Molecular Cell in August of 2015, which is attached to this Final Report as an Appendix. The data above in Figure 1 of this final report will be included in a future publication.

2. Dr. Shaw has given talks on the outcome of this research at the LAM (Lymphangioleiomyomatosis) Conference in Chicago, IL in March 2014, the DFHCC Symposium on Hamartoma syndromes and cancer biology in Boston, MA in May 2015, and the FASEB Protein Kinases and Phosphorylation Meeting in Itsaca, IL in July 2015.

3. We also filed a published patent with the U.S. Patent Office as described:
PCT Application: PCT/US2015/046777
PCT Patent Title: Novel ULK1 Inhibitors and Methods Using Same
Filing Date: 08/25/2015
Inventors: Reuben Shaw, Nicholas Cosford, Daniel Egan, Dhanya Panickar, Benjamin Turk, Mitchell Vamos, Matthew Gee Hong Chun, Doug Sheffler
Status: Published

CONCLUSION:

In this body of work, we have accomplished nearly all of the original stated goals of the grant proposal. Most importantly, we have identified and reported 10 new ULK1 phosphorylation sites and generated a novel phosphor-specific antibody that we used to screen for selective ULK1 inhibitors in cells. This led us to the discovery and refinement of a highly selective small molecular inhibitor of ULK1, SBI-0206965, which we reported in a Molecular Cell paper in August 2015. Since that time, this compound has taken off in the scientific world as the most selective ULK1 inhibitor to date, fueling many new studies from many labs around the world. Meantime, our laboratory continues to explore the use of SBI-0206965 as a

potential therapeutic for TSC. This will be a major focus of the next 3 years of research in my laboratory.

"So what": We have discovered and developed a novel chemical compound which selectively targets a pathway – the ULK1 autophagy pathway – upregulated in TSC patients being treated with rapamycin. Our studies to date suggest this compound SBI-0206965 or derivatives of it may make very effective combination treatments for those with TSC. We aim to begin testing this as soon as possible in animal models and human TSC cell lines. As it states in a press article in the journal *Cancer Discovery* written after our Egan et al. *Molecular Cell* paper came out: "**Impact:** SBI-0206965 may overcome therapeutic resistance in patients treated with mTOR inhibitors."

REFERENCES

Joo, J.H., Dorsey, F.C., Joshi, A., Hennessy-Walters, K.M., Rose, K.L., McCastlain, K., Zhang, J., Iyengar, R., Jung, C.H., Suen, D.F., et al. (2011). Hsp90-Cdc37 chaperone complex regulates Ulk1- and Atg13-mediated mitophagy. *Molecular Cell 43*, 572–585.

Joo, J. H., Wang, B., Frankel, E., Ge, L., Xu, L., Iyengar, R., et al. (2016). The Noncanonical Role of ULK/ATG1 in ER-to-Golgi Trafficking Is Essential for Cellular Homeostasis. *Molecular Cell*, *62*(6), 491-506.

Egan, D.F., Chun, M.G., Vamos, M., Zou, H., Rong, J., Miller, C.J., Lou, H.J., Raveendra-Panickar, D., Yang, C.C., Sheffler, D.J., et al. (2015). Small Molecule Inhibition of the Autophagy Kinase ULK1 and Identification of ULK1 Substrates. *Molecular Cell 59*, 285–297.

APPENDICES

Shaw CV
Bibliography
Egan et al (2015) Molecular Cell journal publication
List of personnel receiving pay from the research effort

General Information

Reuben J. Shaw
William R. Brody Chair
Professor, Molecular and Cell Biology Laboratory
Director, Salk NCI-Designated Cancer Center
The Salk Institute for Biological Studies
10010 North Torrey Pines Road, La Jolla, CA 92037

Education

09/89-06/93	B.S. Biology, Cornell University, Ithaca, NY, *with highest honors*
09/93-06/99	Ph.D. Biology, Massachusetts Institute of Technology, Cambridge, MA

Research Experience/ Training

1991-1993	Undergraduate research, Cornell University	Advisor: Dr. Richard Cerione, Ph.D.
1994-1999	Ph.D., Massachusetts Institute of Technology	Advisor: Dr. Tyler Jacks, Ph.D.
1999-2003	Postdoctoral fellow, Harvard Medical School	Advisor: Dr. Lewis Cantley, Ph.D.
2003-2005	Instructor, Harvard Medical School	Advisor: Dr. Lewis Cantley, Ph.D.
2006-2012	Assistant Professor, Salk Institute	Molecular & Cell Biology Laboratory
2012-2014	Associate Professor, Salk Institute	Molecular & Cell Biology Laboratory
2014-present	Professor, Salk Institute	Molecular & Cell Biology Laboratory

Honors and Awards

2006-2009	The V Foundation for Cancer Research Scholar Award
2007-2011	American Cancer Society Research Scholar
2008-2011	American Diabetes Association Junior Faculty Award
2009-2015	Howard Hughes Medical Institute Early Career Scientist Award

Additional Institutional Affiliations

2006-2016	Assistant Adjunct Professor, Division of Biological Sciences, UCSD
2009-2016	Assistant Adjunct Professor, Department of Medicine, UCSD
2016-present	Adjunct Full Professor, Division of Biological Sciences and Department of Medicine, UCSD

Institutional Service

2006-present	Teach UCSD undergrads and grad courses ~ 5 lectures / year, these committees
2008-2013	Salk Academic Council
2009-present	Developed and run Salk Cancer Course for T32 NCI Cancer Center training grant
2011-present	Developed and run upperclassman / masters / Ph.D. student UCSD course BGGN245
2011-present	Salk Faculty Development Committee
2014-present	UCSD-Salk Ph.D. Graduate Committee
2015-present	Salk Appointments Committee
2013-2015	Associate Program Leader, Salk NCI-Designated Basic Cancer Center
2014-2015	Deputy Director, Salk NCI-Designated Basic Cancer Center
2016-present	Director, Salk NCI-Designated Basic Cancer Center

Extramural Professional Responsibilities

2007-present	Adhoc Manuscript Reviewer: Nature, Cell, Science, Nature Medicine, Nature Cell Biology, Molecular Cell, Cell Metabolism, Cancer Cell, Cell Stem Cell, G&D, JCI, Science Signaling, Elife, MCB, PNAS, PLOS, JBC, Cancer Research, Biochemical Journal, and Oncogene

2009-2012 Member, Grant Review Board, State of Texas Cancer Research Initiative (CPRIT)
2010-2015 Editorial Board, *Oncogene;* Editorial Board, *Biochemical Journal*
2015-present Editorial Board, *Science Signaling*
2009-present Grant Reviewer: NIH (NCI, NIDDK), American Cancer Society, Tuberous Sclerosis Alliance

Meeting Co-organizer:

2009 AACR Meeting on Cancer & Metabolism (w/ Ron Evans & Celeste Simon)
2009 Salk Cancer Mechanisms & Models (w/ Jan Karlseder, Laura Attardi, Clodagh O'Shea & Dave Tuveson)
2011 Salk Cancer Mechanisms & Models (w/ Jan Karlseder, Laura Attardi, Clodagh O'Shea & Dave Tuveson)
2012 Keystone Meeting on Cancer Metabolism (w/ David Sabatini)
2013 FASEB Meeting on Protein Kinase and Protein Phosphorylation (w/ Richard Marais)
2013 Salk Cancer Mechanisms & Models (w/ Jan Karlseder, Laura Attardi, Clodagh O'Shea & Dave Tuveson)
2015 Salk Cancer Mechanisms & Models (w/ Jan Karlseder, Laura Attardi, Clodagh O'Shea & Dave Tuveson)
2016 Salk Post-Translation Regulation of Cell Signaling (w/ Tony Hunter & Alexandra Newton)
2017 Keystone Meeting on Tumor Metabolism (w/ Brendan Manning & Kathryn Wellen)

Invited Talks Given

2016: Invited talks: U of Toronto Endocrine Grand Rounds; Keystone Tumor Metabolism Meeting; Keystone Mitochondrial Dynamics Meeting; IPSEN Cancer Meeting on Tumor Metabolism; NYAS Cancer Metabolism Symposium, AACR Annual Meeting; ADA Annual Meeting; NCI Cancer Center Directors Conclave; ISREC/ EPFL Lola & John Grace Distinguished Lecture in Cancer Research; CSHL Quantitative Symposium on Cancer; Virginia Commonwealth Cancer Biology Dept seminar; CSHL PI3K and mTOR signaling Meeting; International AMPK meeting; Montepelier Metabolism & Cancer 2016 Meeting; University of Alberta CRINA Leaders in Cancer seminar

2015: Invited talks: Keystone Tumor Metabolism Meeting; Keystone Metabolic Disease and Mitochondrial Dysfunction Meeting; NIH Tuberous Sclerosis Workshop; NCI Cancer Center Directors Conclave; UCLA Tumor Metabolism Symp; AACR Annual Meeting; U Iowa Physiology Dept Seminar, U Chicago Cancer Biology Dept Seminar, UPenn Institute for Diabetes, Obesity, and Metabolism Seminar; Harvard Med Harmatoma Tumor Suppressors Symposium; AACR Cancer Metabolism Mtg; Cell Press Mitochondria Symposium; FASEB Kinase Mtg; FASEB HDAC Meeting; 78th Harden Conference, 40th European Symp on Hormones and Cell Regulation; Arias Liver Symposium; UMass Med School Molecular Cell / Cancer Biology Dept Seminar; Banbury Tumor Metabolism Mtg

2014 Invited talks: CSHL Pten Meeting; LAM Symposium 2014; AACR Annual Meeting; Abcam meeting on Epigenetics and Metabolism; BMC Metabolism, Diet, and Disease, Lewis Cantley 65th Symposium at Harvard Medical School, Beatson Institute Meeting on Driving the Cancer Engine, FASEB Phosphorylation Meeting, FASEB Nutrient Sensing Meeting, FASEB International AMPK Meeting, AACR International Mtg in Shanghai, TSC International Mtg 2014 Beijing, Baylor MCB Dept, Houston Health Science Center, St. Jude Biomedical Sciences Symposium 2014, University of Leuven Second Annual Metabolism Symposium, EMBO|EMBL Symposium on Frontiers in Metabolism

2013 Other invited talks given beyond meetings I co-organized: 25th Pezcoller Symposium Trento Italy Banbury Meeting on Biguanides, CSHL meeting on Metabolism & Disease, Yale University Physiology Dept, Memorial Sloan-Kettering Cancer Center, Oregon Health Science University, Keystone Tumor Metabolism Meeting, Annual AACR meeting, World Congress on Insulin Resistance, Diabetes & Cardiovascular Disease

2012 Other invited talks given beyond meetings I co-organized: Banbury Meeting on Cancer Metabolism, Les Treilles TOR Meeting, St. Jude's 50th Anniversary Symposium, annual Forbeck Symposium, FASEB Meeting on AMPK, EPFL School of Life Sciences, London Research Institute, IPSEN Cancer Meeting on Mouse Models, Albert Einstein Cell Biology Dept, Dartmouth Medical School, annual American Diabetes Association Meeting, annual Endocrine Society Meeting

2011 Other invited talks given beyond meetings I co-organized: CSHL 76th Annual Symposium on Metabolism & Disease, Molecular and Physiological Aspects of Type 2 Diabetes and Obesity Symposium at the Karolinska Institute, Keystone Diabetes Meeting, Aspen Cancer Conference, FASEB Meeting on Kinases and Protein Phosphorylation, FASEB Meeting on Nutrient Control and Metabolism, AACR Meeting on Metabolism and Cancer, Banbury Meeting on Metformin and Cancer, University of Utah Metabolism Symposium, Washington University Cell Biology Dept, University of Pennsylvania Cancer Center, Stanford Cancer Center, McGill Cancer Center, Massachusetts General Hospital Cancer Center, UTSW Children's Hospital Cancer Institute

2010 Invited talks: American Association of Cancer Research (AACR) Annual Meeting, Metabolism in Cancer Conference, Berlin, Germany, Gordon Conference on Cell Growth and Proliferation, The tumor suppressor LKB1: basic science to the clinic in Marseilles France, FASEB 5th International AMPK Conference in Kyoto; Keystone Meeting on Cancer & Metabolism, CSHL PTEN meeting, Fred Hutchinson Cancer Center, Dana Farber Cancer Center, CSHL 5th Annual Cancer Mechanisms & Models, Abcam Cancer and Metabolism Meeting, Banbury Meeting on Cancer Metabolism, Barcelona Biomed Conference on Cancer Metabolism, Vanderbilt Weekly Physiology Seminar Series, NCI Workshop on Cancer and Autophagy

2009 Other invited talks given at meeting or weekly seminar series: CNIO Meeting on Cancer and Metabolism, American Cancer Society Professors Meeting, Abcam Meeting on Aging and Age-related disease, FASEB Meeting on Kinases and Protein Phosphorylation, Duke University Department of Pharmacology, Case Western University Dept of Pathology, Forbeck Foundation Annual Meeting, Tuberous Sclerosis Alliance International Symposium, UCLA IMED Seminar Series, Yale Medical School Pharmacology Weekly Seminar, Memorial Sloan-Kettering Cancer Center Cancer Biology weekly Seminar

2008 Other invited talks: American Association of Cancer Research (AACR) Annual Meeting, CNIO Cancer Conference on mTOR Signaling Metabolism & Cancer, CSHL 3rd Annual Cancer Mechanisms & Models, FASEB Meeting on Nutrient Regulation, FASEB International AMPK Meeting in Copenhagen, IPSEN Cancer and Metabolism Meeting, Minisymposium at Fred Hutchinson Cancer Research Center, Beatson Institute Cancer & Metabolism Symposium, UNC Lineberger Comprehensive Cancer Center Weekly Seminar, Boston Medical Center Whittaker Cardiovascular Weekly Seminar, Annual LAM (Lymphoangiomyoleiosarcoma) Foundation Meeting, UC Irvine Molecular and Cell Biology Weekly Seminar, UT Southwestern Pathology Weekly Seminar, UT Southwestern Pharmacology Weekly Seminar, UPenn Mari Lowe Center for Comparative Oncology Weekly Seminar, National Cancer Institute Distinguished Scientist Lecture

2007 Other invited talks: Gordon Conference on Signaling in the Nucleus, Keystone Symposium on Nuclear Receptor Pathways and Metabolic Syndrome, American Association of Cancer Research Annual Meeting, American Diabetes Association Annual Meeting, Gordon Conference on Cell Growth & Proliferation, FASEB Meeting on Protein Kinases, Kern Lipid Conference, UCLA Hillblom Diabetes Symposium on Tumor Suppressors and Diabetes, UC Davis Cancer Center Weekly Seminar, UCSD Mahajani Symposium on Cancer & Metabolism, International Tuberous Sclerosis Alliance Annual Meeting, University of Wisconsin at Madison Weekly Seminar

2006 Keystone Diabetes Meeting, Nutrient Sensing, NCI Insulin Signaling and Hamartoma Syndromes Meeting, UCSF Cancer Center, Gordon Conference on Phosphorylation & G Protein Mediated Signaling, FASEB Meeting on AMPK, Annual Obesity Society Conference

Shaw Lab Personnel - December 2015

11 postdoctoral fellows, 3 PhD students, 3 research technicians

Former Trainees

1st postdoc David Shackelford finished 2011, now an Assistant Professor at UCLA Medical School
Will Mair, a joint postdoc with Andrew Dillin finished 2011, now Asst Prof at Harvard School of Public Health
Jung-Whan (Jay) Kim, joint postdoc with Randy Johnson finished 2013, now Asst Prof at UT Dallas
1st PhD student Dana Gwinn is now a postdoc at Stanford
2nd PhD student Maria Mihaylova is now a postdoc at the Whitehead Institute at MIT
3rd PhD student Rebecca Kohnz is now a postdoc at UC Berkeley.
4th PhD student Daniel Egan is now a postdoc at Harvard Medical School
5th PhD student Jonathan Goodwin is now a postdoc at Novartis in Boston

Publications – Primary Research

1. Young, N.P., Reddy, A., Van Nostrand, J.L., Eichner, L.J., Shokhirev, M.H., Dayn, Y., and **Shaw, R.J**. (2016) AMPK governs lineage specification through Tfeb-dependent regulation of lysosomes. ***Genes & Dev,*** *30:* 535–552

2. Toyama, E.Q., Herzig, S., Courchet, J., Lewis, T.L. Jr., Losón, O.C., Hellberg, K., Young, N.P., Chen, H., Polleux, F., Chan, D.C., and **Shaw, R.J**. (2016) AMP-activated protein kinase mediates mitochondrial fission in response to energy stress. ***Science*** *351:* 275-281

3. Schaffer, B.E., Hertz, N.T., Levin, R.S., Maures, T.J., Schoof, M.L., Hollstein, P.E., Benayoun, B.A., Banko, M.R., **Shaw, R.J.**, Shokat, K.M., Brunet, A. (2015) Identification of AMPK phosphorylation sites reveals a network of proteins involved in cell invasion and facilitates large-scale substrate prediction. ***Cell Metab*** 22 :907-21

4. McClatchy DB, Ma Y, Liu C, Stein BD, Martínez-Bartolomé S, Vasquez D, Hellberg K, **Shaw R.J.**, Yates JR 3rd. (2015) Pulsed Azidohomoalanine Labeling in Mammals (PALM) Detects Changes in Liver-Specific LKB1 Knockout Mice. ***J Proteome Res.*** 14:4815-22

5. Egan, D.F., Chun, M.G., Vamos, M., Zou, H., Rong, J., Miller, C.J., Lou, H.J., Raveendra-Panickar, D., Yang, C.C., Sheffler, D.J., Teriete, P., Asara, J.M., Turk, B.E., Cosford, N.D. and, **Shaw, R.J.** (2015). Small molecule inhibition of the autophagy kinase ULK1 and identification of ULK1 substrates. ***Molecular Cell*** 59: 285–297

6. Goodwin, J.M., Svensson, R.U., Lou, H.J., Winslow, M.M., Turk, B.E., and **Shaw, R.J.** (2014). An AMPK-Independent Signaling Pathway Downstream of the LKB1 Tumor Suppressor Controls Snail1 and Metastatic Potential. ***Molecular Cell*** 55: 436–450.

7. Luan, B., Goodarzi, M.O., Phillips, N.G., Guo, X., Chen, Y.I., Yao, J., Allison, M., Rotter, J.I., **Shaw, R.J**., and Montminy, M. (2014) Leptin-mediated increases in Catecholamine signaling reduce adipose tissue inflammation via activation of Macrophage HDAC4. ***Cell Metab*** 19:1058-65.

8. Faubert, B., Vincent, E.E., Griss, T., Samborska, B., Izreig, S., Svensson, R.U., Mamer, O.A., Avizonis, D., Shackelford, D.B., **Shaw, R.J.**, and Jones, R.G. (2014) Loss of the tumor suppressor LKB1 promotes metabolic reprogramming of cancer cells via HIF-1a. ***Proc Natl Acad Sci USA*** 111: 2554-2559.

9. Masui, K., Tanaka, K., Akhavan, D., Babic, I., Gini, B., Matsutani, T., Iwanami, A., Liu, F., Villa, G.R., Gu, Y., Campos, C., Zhu, S., Yang, H., Yong, W.H., Cloughesy, T.F., Mellinghoff, I.K., Cavenee, W.K., **Shaw, R.J**., and Mischel, P.S. (2013) mTOR Complex 2 Controls Glycolytic Metabolism in Glioblastoma through FoxO Acetylation and Upregulation of c-Myc. ***Cell Metab*** 18: 726-739.

10. Liu, Y., Marks, K., Cowley, G.S., Carretero, J., Liu, Q., Nieland, T.J., Xu, C., Cohoon, T.J., Gao, P., Zhang, Y., Chen, Z., Altabef, A.B., Tchaicha, J.H., Wang, X., Choe, S., Driggers, E.M., Zhang, J., Bailey, S.T., Sharpless, N.E., Hayes, D.N., Patel, N.M., Janne, P.A., Bardeesy, N., Engelman, J.A., Manning, B.D., **Shaw, R.J.,** Asara, J.M., Scully, R., Kimmelman, A., Byers, L.A., Gibbons, D.L., Wistuba, I.I., Heymach, J.V., Kwiatkowski, D.J., Kim, W.Y., Kung, A.L., Gray, N.S., Root, D.E., Cantley, L.C., and Wong, K.K. (2013) Metabolic and functional genomics identify deoxythymidylate kinase as a target in LKB1-mutant lung cancer. ***Cancer Discov*** 3: 870-879.

11. Shackelford, D.B, Abt, E., Gerken, L., Vasquez, D.S., Seki, A., Leblanc, M., Wei, L., Fishbein, M.C., Czernin, J., Mischel, P.S., and **Shaw, R.J**. (2013) LKB1 inactivation dictates therapeutic response of non-small cell lung cancer to the metabolism drug phenformin. ***Cancer Cell*** 23: 143-158.

12. Xia, Y., Yeddula, N., LeBlanc, M., Ke, E., Zhang, Y., Oldfield, E., **Shaw, R.J**., and Verma, I.M. (2012) Reduced cell proliferation by IKK2 depletion in a mouse lung-cancer model. ***Nat Cell Biol*** 14: 257-265.

13. Auricchio, N., Malinowska, I., **Shaw, R.**, Manning, B.D., and Kwiatkowski, D.J. (2012). Therapeutic trial of metformin and bortezomib in a mouse model of tuberous sclerosis complex (TSC). ***PLoS One*** 7:e31900.

14. Wang, B., Moya, N., Niessen, S., Hoover, H., Mihaylova, M.M., **Shaw, R.J.**, Yates, J.R. 3rd, Fischer, W.H., Thomas, J.B. and Montminy, M. (2011) A hormone-dependent module regulating energy balance. ***Cell*** 145:596-606.

15. Mihaylova, M.M., Vasquez, D.S., Ravnskjaer, K., Denechaud, P.D., Yu. R.T., Alvarez, J.G., Downes, M., Evans. R.M., Montminy, M., and **Shaw, R.J.** (2011) Class IIa histone deacetylases are hormone-activated regulators of FOXO and mammalian glucose homeostasis. ***Cell*** 145: 607-621.

16. Li, Y., Xu, S., Mihaylova, M., Zheng, B., Hou, X., Jiang, B., Park, O.,Luo, Z., Lefai, E., Shyy, J.Y., Gao, B., Wierzbicki, M., Verbeuren, T.J., **Shaw, R.J.**, Cohen, R.A., and Zang, M. (2011) AMPK Phosphorylates and Inhibits SREBP Activity to Attenuate Hepatic Steatosis and Atherosclerosis in Diet-induced Insulin Resistant Mice. ***Cell Metab*** 13: 376-388.

17. Mair, W., Morantte, I., Rodrigues, A.P., Manning, G., Montminy, M., **Shaw, R.J.*** and Dillin, A.* (2011) Lifespan extension induced by AMPK and calcineurin is mediated by CRTC-1 and CREB. ***Nature*** 470:404-408. *(*co-corresponding authors)*

18. Egan, D.F., Shackelford, D.B., Mihaylova, M.M., Gelino, S.R., Kohnz, R.A., Mair, W., Vasquez, D.S., Joshi, A., Gwinn, D.M., Taylor, R., Asara, J.M., Fitzpatrick, J., Dillin, A., Viollet, B., Kundu. M., Hansen, M. and **Shaw, R.J.** (2010) Phosphorylation of ULK1 (hATG1) by AMP-Activated Protein Kinase Connects Energy Sensing to Mitophagy. ***Science*** 331: 456-461.

19. Gwinn, D.M., Asara, J. and **Shaw, R.J.** (2010) Raptor is phosphorylated by cdc2 during mitosis. ***PLoS ONE*** 5: e9197.

20. Ohashi, K., Ouchi, N., Higuchi, A., **Shaw, R.J.,** and Walsh**,** K. (2010) LKB1 deficiency in Tie2-Cre expressing cells impairs ischemia-induced angiogenesis. ***J Biol Chem*** 285: 22291-22298.

21. Ikeda, Y., Sato, K., Pimentel, D.R., Sam, F., **Shaw, R.J**., Dyck, J.R., Walsh, K. (2009) Cardiac-specific deletion of LKB1 leads to hypertrophy and dysfunction. ***J Biol Chem*** 284: 35839-35849.

22. Lamia, K.A., Sachdeva, U.M., DiTacchio, L., Williams, E.C., Alvarez, J.G, Egan, D.F., Vasquez, D.S., Juguilon, H., Panda, S., **Shaw, R.J**., Thompson, C.B., and Evans, R.M. (2009) AMPK regulates the circadian clock by cryptochrome phosphorylation and degradation. ***Science*** 326: 437-440.

23. Shackelford, D.B., Vasquez, D.S., Corbeil, J., Wu, S., Leblanc, M., Wu, C.-L., Vera, D.R. and **Shaw, R.J**. (2009) mTOR and HIF-1α mediated tumor metabolism in an LKB1 mouse model of Peutz-Jeghers syndrome. ***Proc Natl Acad Sci USA*** 106: 11137-11142.

24. Mair, W., Panowski, S.H., **Shaw, R.J.**, and Dillin, A. (2009) Optimizing Dietary Restriction for Genetic Epistasis Analysis and Gene Discovery in C. elegans. ***PLoS One***, 4: e4535.

25. Narkar, V.A., Downes, M., Yu, R.T., Embler, E., Wang, Y.X., Banayo, E., Mihaylova, M.M., Nelson, M.C., Zou, Y., Juguilon, H., Kang, H., **Shaw, R.J.** and Evans, R.M. (2008) AMPK and PPARdelta agonists are exercise mimetics. ***Cell*** 134: 405-415.

26. Gwinn, D.M., Shackelford, D.B., Egan, D.F., Mihaylova, M.M., Mery, A., Vasquez, D.S., Turk, B.E. and **Shaw, R.J.** (2008) AMPK phosphorylation of raptor mediates a metabolic checkpoint. ***Mol Cell*** 30: 214-226.

27. Baur, J.A., Pearson, K.J., Price, N.L., Jamieson, H.A., Lerin, C., Kalra, A., Prabhu, V.V., Allard, J.S., Lopez-Lluch, G., Lewis, K., Pistell, P.J., Poosala, S.Becker, K.G., Boss, O., Gwinn, D., Wang, M., Ramaswamy, S., Fishbein, K.W., Spencer, R.G., Lakatta, E.G., LeCouteur, D., **Shaw, R.J**., Navas, P., Puigserver, P., Igram, D.K., deCabo, R., Sinclair, D.A. (2006) Resveratrol improves health and survival of mice on a high-calorie diet. ***Nature*** 444: 337-342.

28. **Shaw, R.J**.*, Lamia, K.A., Vasquez, D., Koo, S.H., Bardeesy, N., DePinho, R.A., Montminy, M., Cantley, L.C. (2005) The Kinase LKB1 Mediates Glucose Homeostasis in Liver and Therapeutic Effects of Metformin. ***Science*** 310: 1642-1646. (**corresponding author)*

29. Fernandes, N., Sun, Y., Chen, S., Paul, P., **Shaw, R.J**., Cantley, L.C., Price, B.D. (2005) DNA damage-induced association of ATM with its target proteins requires protein interaction domain in the N terminus of ATM. ***J Biol Chem*** 280:15158-15164.

30. **Shaw, R.J**., Bardeesy, N., Manning, B., Lopez, L. Kosmatka, M., DePinho, R.A., and Cantley, L.C. (2004) The LKB1 tumor suppressor negatively regulates mTOR signaling. ***Cancer Cell*** 6: 91-99.

31. **Shaw, R.J**., Kosmatka, M., Bardeesy, N., Hurley, R.L., Witters, L.A., DePinho, R.A., Cantley, L.C. (2004) The tumor suppressor LKB1 kinase directly activates AMP-activated kinase and regulates apoptosis in response to energy stress. ***Proc Natl Acad Sci USA*** 101: 3329-3335.

32. Karuman, P., Gozani, O., Odze, R., Zhou, X.C., Zhu, H., **Shaw, R.**, Brien, T.P., Bozzuto, C.D., Ooi, D., Cantley, L.C., and Yuan, J . (2001) The Peutz-Jegher Gene Product LKB1 is a mediator of p53- dependent cell death. ***Mol Cell*** 7: 1307-1319.

33. **Shaw, R.J.**, Paez, J.G., Curto, M., Yaktine, A., Pruitt, W.M., Saotome, I., O'Bryan, J.P., Gupta, V., Ratner, N., Der, C.J., Jacks, T. and McClatchey, A.I. (2001) The Nf2 tumor suppressor, merlin, functions in Rac-dependent signaling. ***Dev Cell*** 1: 63-72.

34. **Shaw, R.J.**, McClatchey, A.I., and Jacks, T. (1998) Regulation of the Neurofibromatosis type 2 tumor suppressor protein, merlin, by adhesion and growth arrest stimuli. ***J Biol Chem*** 273: 7757-64.

35. **Shaw, R.J**., McClatchey, A.I., and Jacks, T. (1998) Localization and functional domains of the Neurofibromatosis type II tumor suppressor, merlin. ***Cell Growth Diff*** 9: 287-296.

36. **Shaw, R.J.**, Henry, M., Solomon, F., and Jacks, T. (1998) RhoA-dependent phosphorylation and re-localization of ERM proteins into apical membrane/ actin protrusions in fibroblasts. ***Mol Biol Cell*** 9:403-19.

37. Platko, J., Leonard, D., Adra, C., **Shaw, R.J**., and Cerione, R.A. (1995) A single residue can modify target binding affinity and activity of the functional domain of the Rho-subfamily GDP dissociation inhibitors. ***Proc Natl Acad Sci USA*** 92: 2974-2978.

Publications – Reviews, Essays, Previews, Book Chapters, etc.

1. Garcia, D. and **Shaw, R.J.** (2016) AMPK: central responder to mitochondrial damage. ***Trends in Biochem Sci*** [*in press]*

2. Svensson, R.U. and **Shaw, R.J.** (2016) The AMPK pathway: a starvation pathway keeping some tumors alive and killing other tumors off ***Nature Rev Cancer*** [*in press]*

3. **Shaw, R.J.** (2015) AMPK Keeps Tumor Cells from Starving to Death. ***Cell Stem Cell*** 17, 503-4.

4. **Shaw, R.J.** (2015) Tumor Metabolism: MAGE-A Proteins Help TRIM Turnover AMPK. ***Curr Biol*** 25: R418

5. Mouchiroud, L., Eichner, L.J., **Shaw, R.J**, and Auwerx, J. (2014) Transcriptional coregulators: fine-tuning metabolism. ***Cell Metab*** 20: 26-40.

6. **Shaw, R.J.** (2013) Metformin trims fats to restore insulin sensitivity. ***Nat Med*** 19: 1570-1572.

7. **Shaw, R.J.** (2013) GATORs take a bite out of mTOR. ***Science***. 340: 1056-1057.

8. Chun, M.G. and **Shaw, R.J.** (2013) Cancer metabolism in breadth and depth. ***Nat Biotech*** 31: 505-507.

9. Mihaylova, M.M. and **Shaw, R.J**. (2013) Metabolic Reprogramming by Class I and II histone deacetylases. ***Trends Endo Metab*** 24: 48-60.

10. Svensson, R.U. and **Shaw, R.J.** (2012) Cancer metabolism: tumor friend or foe. ***Nature*** 485: 590-591.

11. **Shaw, R.J.** and Cantley, L.C. (2012) Cell biology: ancient sensor for ancient drug. ***Science*** 336: 813-814.

12. **Shaw, R.J.** and Cantley, L.C. (2012) Decoding key nodes in the metabolism of cancer cells: sugar & spice and all things nice. ***F1000 Reports*** 4: 2. (doi:10.3410/B4-2)

13. Mihaylova, M.M. and **Shaw, R.J.** (2011) The AMPK signalling pathway coordinates cell growth, autophagy, and metabolism. ***Nat Cell Biol*** 13: 1016-1023.

14. Akhtar, A., Fuchs, E., Mitchison, T., **Shaw, R.J.**, St. Johnston, D., Strasser, A., Taylor, S., Walczak, C., Zerial, M. (2011) A decade of molecular cell biology: achievements and challenges. ***Nat Rev Mol Cell Biol*** 12: 669-774.

15. Birnbaum, M.J. and **Shaw, R.J.** (2011) Genomics: Drugs, diabetes, and cancer. ***Nature*** 470: 338-339.

16. Egan, D., Kim, J., **Shaw, R.J.**, and Guan, K.L. (2011) The autophagy initiating kinase ULK1 is regulated via opposing phosphorylation by AMPK and mTOR. ***Autophagy*** 7: 643-644.

17. Gwinn, D.M. and **Shaw, R.J**. (2010) AMPK control of mTOR signaling and growth. ***The Enzymes.*** Chapter 3, pp.49-75.

18. **Shaw, R.J.**, Evans,R.M.,Simon, M.C. (2010) Metabolism and cancer in La Jolla. ***Cancer Res*** 70: 3864-9.

19. **Shaw, R.J.** (2010) Metabolism and cancer mix in Madrid. ***EMBO Rep*** 11: 249-251.

20. Shackelford, D.B. and **Shaw, R.J.** (2009) The LKB1-AMPK pathway: metabolism and growth control in tumour suppression. ***Nat Rev Cancer*** 9: 563-575.

21. Mihaylova, M.M. and **Shaw, R.J.** (2009) AMPK: Central Regulator of Glucose and Lipid Metabolism. ***The Liver: Biology and Pathobiology***, 5th edition, Wiley-Blackwell, pp.535-549.

22. **Shaw, R.J**. (2009) LKB1 and AMP-activated protein kinase control of mTOR signalling and growth. ***Acta Physiol*** 196: 65-80.

23. **Shaw, R.J.** (2009) Tumor suppression by LKB1: SIK-ness prevents metastasis. ***Sci Signaling*** 1: pe65

24. **Shaw, R.** and Dillin, A. (2009) PPTR-1 counterAkts insulin signaling. ***Cell*** 136: 816-818.

25. **Shaw, R.J.** and Cantley, L.C. (2008) The PI3K-LKB1 Pathway. Inborn Errors of Development. 2nd Edition. Epstein CJ, Erickson RP, Wynshaw-Boris A, editors. Oxford, UK: ***Oxford University Press.*** Chapter 57, p.273-279.

26. **Shaw, R.J.** (2008) Raptor swoops in on metabolism. ***Cell Metab*** 8: 343-344.

27. **Shaw, R.J.** (2008) LKB1: cancer, polarity, metabolism, and now fertility. ***Biochem J*** 416: e1-3.

28. **Shaw, R.J.** (2008) mTOR signaling: RAG GTPases transmit the amino acid signal. ***Trends Biochem Sci*** 33: 565-568.

29. **Shaw, R.J.** (2006) Glucose metabolism and cancer. ***Curr Opin Cell Biol*** 18*:* 598-608.

30. **Shaw, R.J.** and Cantley, L.C. (2006) Ras, PI3(K), and mTOR signaling control tumor cell growth. ***Nature*** 441: 424-430.

D. Research Support

ONGOING

5 P30 CA014195-43 (Shaw, PI) 12/01/2014-11/30/2018
NIH/NCI
Cancer Center Support Grant
The major goal of this project is to understand fundamental aspects of biology related to cancer, with the ultimate goal of reducing cancer incidents, morbidity and mortality.
Role: Director, Cancer Center, 01/01/16

5 P01 CA120964-09 (Kwiatkowski, PI) 09/21/2012-07/31/2017
NIH/NCI
Molecular Pathogenesis of the Hamartoma Syndromes
The major goal of Project 2, LKB1/AMPK Signaling and Peutz-Jeghers Syndrome (L. Cantley, Project Leader, R. Shaw, Project Co-Leader), is to gain a detailed understanding of the LKB1-AMPK signaling network so that we can design therapeutic approaches to selectively attack tumors that emerge in patients with either germline or sporadic mutations in LKB1.
Role: Co-Investigator

4 R01 CA172229-04 (Shaw, PI) 01/16/2013-12/31/2017
NIH/NCI
AMPK and AMPK-related kinases in lung cancer development and treatment
The major goal of this project is to decode the critical tumor suppressor functions and downstream components of a cancer-causing biochemical pathway that is amongst the most frequently mutated in human lung cancer.
Role: PI

5 R01 DK080425-09 (Shaw, PI) 07/01/2012-06/30/2017
NIH/NIDDK
LKB1-AMPK pathway regulation of glucose metabolism and metformin action in liver
The major goal of this project is to further dissect the role of AMPK and its related SIK family kinases in control of hepatic metabolism and therapeutic action of metformin in mouse models.
Role: PI

COMPLETED

W81XWH-13-1-0043 (Shaw, PI) 04/01/2013-03/31/2016
Department of Defense
Defining the role of autophagy kinase ULK1 signaling in therapeutic response of Tuberous Sclerosis Complex to mTOR inhibitors
The major goal of this project is to test how inhibition of ULK1 may change the normally cytostatic effect of rapalogs and other mTOR catalytic inhibitors in TSC-deficient cells into a cytotoxic effect.
Role: PI

W81XWH-13-1-0105 (Metallo, PI) 06/01/2014-05/31/2015
Department of Defense
Targeting Metabolic Survival Pathways in Lung Cancer via Combination Therapy
The major goal of this project is to examine the control of metabolism by the LKB1-AMPK pathway. We will design and analyze the xenograft tumor model studies; this involves treating mice bearing non-small cell lung cancer xenografts with combinations of therapeutics targeting the metabolism of the tumors.
Role: Co-Investigator

Early Career (Shaw, PI) 09/15/2009-08/31/2015
Howard Hughes Medical Institute
Nutrient-Sensing Signaling Pathways Controlling Cancer and Diabetes
The major goal of this project is to elucidate mechanisms by which cells connect nutrient availability to cell growth and metabolism.
Role: PI

Research Grant (Evans/Shaw, PI) 07/01/2012-06/30/2013
Samuel Waxman Cancer Research Foundation
Chronic Inflammation and Metabolic Dysregulation in Cancer
The major goal of this project is to provide insight into the molecular mechanisms and the contributing role of inflammation and bile acid homeostasis in diet-induced intestinal cancer, and evaluate a pathway-specific therapeutic approach for cancer treatment.
Role: Co-Investigator

Research Grant (Evans/Shaw, PI) 07/01/2013-06/30/2014
Samuel Waxman Cancer Research Foundation
Dietary stress-induced epigenetic signatures in cancer
The major goal of this project is to understand the consequences of environmental (high fat diet) and genetic (LKB+/-) stressors on specific tissue's propensity for cancer.
Role: Co-Investigator

Research Grant (Evans/Shaw, PI) 07/01/2014-06/30/2015
Samuel Waxman Cancer Research Foundation
Dietary stress-induced epigenetic signatures in cancer
The major goal of this project is to understand the consequences of environmental (high fat diet) and genetic (LKB+/-) stressors on specific tissue's propensity for cancer.
Role: Co-Investigator

BIBLIOGRAPHY

1. Egan, D.F., *et al.* Small molecule inhibition of the autophagy kinase ULK1 and identification of ULK1 substrates. *Mol Cell* **59**, 285–297 (2015).

Article

Molecular Cell

Small Molecule Inhibition of the Autophagy Kinase ULK1 and Identification of ULK1 Substrates

Graphical Abstract

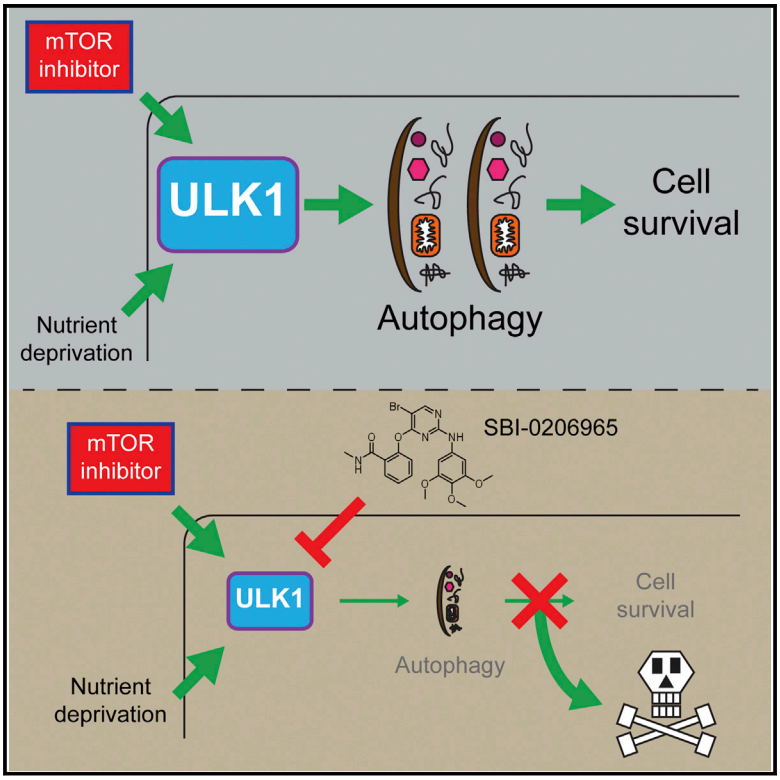

Authors

Daniel F. Egan, Matthew G.H. Chun, Mitchell Vamos, ..., Benjamin E. Turk, Nicholas D.P. Cosford, Reuben J. Shaw

Correspondence

ncosford@sanfordburnham.org (N.D.P.C.), shaw@salk.edu (R.J.S.)

In Brief

ULK1 is a serine/threonine kinase that initiates autophagy in response to nutrient deprivation. Egan et al. define ULK1's consensus phosphorylation motif, demonstrate that ULK1 phosphorylates several autophagy components, and develop a ULK1 small molecule inhibitor (SBI-0206965). SBI-0206965 synergizes with mTOR inhibition to enhance apoptosis in tumor cells, suggesting therapeutic opportunities.

Highlights

- ULK1 phosphorylates multiple autophagy components, including VPS34 on Ser249
- SBI-0206965 is a highly selective ULK1 kinase inhibitor that blocks autophagy
- SBI-0206965 combined with starvation or mTOR inhibition leads to ULK1 degradation
- SBI-0206965 synergizes with mTOR inhibition to induce cell death

Egan et al., 2015, Molecular Cell *59*, 1–13
July 16, 2015
http://dx.doi.org/10.1016/j.molcel.2015.05.031

CellPress

Please cite this article in press as: Egan et al., Small Molecule Inhibition of the Autophagy Kinase ULK1 and Identification of ULK1 Substrates, Molecular Cell (2015), http://dx.doi.org/10.1016/j.molcel.2015.05.031

Molecular Cell
Article

Small Molecule Inhibition of the Autophagy Kinase ULK1 and Identification of ULK1 Substrates

Daniel F. Egan,[1,8] Matthew G.H. Chun,[1,8] Mitchell Vamos,[3] Haixia Zou,[3] Juan Rong,[3] Chad J. Miller,[4] Hua Jane Lou,[4] Dhanya Raveendra-Panickar,[3] Chih-Cheng Yang,[7] Douglas J. Sheffler,[3] Peter Teriete,[3] John M. Asara,[5,6] Benjamin E. Turk,[4] Nicholas D.P. Cosford,[3,*] and Reuben J. Shaw[1,2,*]
[1]Molecular and Cell Biology Laboratory
[2]Howard Hughes Medical Institute
The Salk Institute for Biological Studies, La Jolla, CA 92037, USA
[3]Cell Death and Survival Networks Research Program, NCI-Designated Cancer Center, Sanford-Burnham Medical Research Institute, 10901 North Torrey Pines Road, La Jolla, CA 92037, USA
[4]Department of Pharmacology, Yale University School of Medicine, New Haven, CT 06520, USA
[5]Division of Signal Transduction, Beth Israel Deaconess Medical Center, Boston, MA 02115, USA
[6]Department of Medicine, Harvard Medical School, Boston, MA 02115, USA
[7]Functional Genomics Core, Sanford-Burnham Medical Research Institute, 10901 North Torrey Pines Road, La Jolla, CA 92037, USA
[8]Co-first author
*Correspondence: ncosford@sanfordburnham.org (N.D.P.C.), shaw@salk.edu (R.J.S.)
http://dx.doi.org/10.1016/j.molcel.2015.05.031

SUMMARY

Many tumors become addicted to autophagy for survival, suggesting inhibition of autophagy as a potential broadly applicable cancer therapy. ULK1/Atg1 is the only serine/threonine kinase in the core autophagy pathway and thus represents an excellent drug target. Despite recent advances in the understanding of ULK1 activation by nutrient deprivation, how ULK1 promotes autophagy remains poorly understood. Here, we screened degenerate peptide libraries to deduce the optimal ULK1 substrate motif and discovered 15 phosphorylation sites in core autophagy proteins that were verified as in vivo ULK1 targets. We utilized these ULK1 substrates to perform a cell-based screen to identify and characterize a potent ULK1 small molecule inhibitor. The compound SBI-0206965 is a highly selective ULK1 kinase inhibitor in vitro and suppressed ULK1-mediated phosphorylation events in cells, regulating autophagy and cell survival. SBI-0206965 greatly synergized with mechanistic target of rapamycin (mTOR) inhibitors to kill tumor cells, providing a strong rationale for their combined use in the clinic.

INTRODUCTION

Autophagy is a central cellular mechanism for the elimination of damaged proteins, protein complexes, and organelles. This evolutionarily conserved process plays a crucial role in the cellular response to nutrient deprivation as well as other stresses, in addition to being required for proper cellular and tissue homeostasis during embryonic development and defense against pathogens. Defects in autophagy pathways have been associated with a number of human pathologies, including infectious diseases, neurodegenerative disorders, and cancer (Green and Levine, 2014). In spite of these highly conserved fundamental cellular functions, the molecular and biochemical details of how autophagy is initiated for different cargoes as well as the coordination of steps starting with autophagosome induction to ultimate fusion with the lysosome remain poorly understood.

Pioneering studies in budding yeast first defined 36 core genes required for autophagy, most of which are conserved in mammals (Tsukada and Ohsumi, 1993). One of the most upstream components of the pathway in yeast is the *ATG1* gene, which is notable for being the only core autophagy gene to encode a serine/threonine kinase. Atg1 forms a complex with multiple regulatory subunits, including Atg13 and Atg17. In mammals, there are two Atg1 homologs, ULK1 and ULK2, which similarly bind to an Atg13 homolog and an Atg17-like protein, FIP200 (Chan, 2009). The ULK1 kinase complex is activated in response to nutrient deprivation and serves as a critical initiator of starvation-induced autophagy. It remains unclear if the ULK1 complex is needed for bulk steady-state autophagy that some cell types undergo. Moreover, it has been reported that certain forms of selective autophagy proceed without involvement of the ULK1 complex (Cheong et al., 2011), presumably at least in part via direct signaling to the downstream Vps34/Beclin1 complex.

The requirement for ULK1 in autophagy initiation has been most extensively studied in the context of nutrient deprivation. The mechanistic target of rapamycin complex 1 (mTORC1) is a serine/threonine kinase complex that is inhibited by a wide variety of cellular stresses and as such serves as a central integrator that coordinates cell growth and catabolism under nutrient replete conditions. Studies in *S. cerevisiae*, *D. melanogaster*, and mammalian cells have demonstrated that mTOR acutely inhibits Atg1/ULK1 function through phosphorylation of Atg1/ULK1 and/or some of its associated regulatory subunits (Chan, 2009). Beyond this inhibitory event, ULK1 also receives positive inputs from the cellular energy sensor AMP-activated protein kinase (AMPK), which is activated in response to cellular stresses

that lower intracellular ATP levels, such as is caused by glucose or oxygen deprivation as well as mitochondrial insults (Egan et al., 2011b). While AMPK activates ULK1 by phosphorylating at least four sites (Egan et al., 2011a), mTORC1 inactivates ULK1 by phosphorylating a single site, Ser757 (Kang et al., 2013; Kim et al., 2011). As several physiological stresses result in both AMPK activation and mTOR inhibition, ULK1 activation proceeds through positive signals from AMPK and loss of inhibitory signals from mTORC1 (Egan et al., 2011a). It is notable, however, that mTORC1 is inactivated by many stresses beyond just those affecting AMPK, and the data to date suggest that pharmacological suppression of mTORC1 is sufficient to induce ULK1 kinase activity (Russell et al., 2013).

While mTOR inhibitors have been proposed as general anti-cancer agents due to the requirement of mTOR signaling for cell growth in most tumor settings, it is notable that mTOR inhibitors are largely cytostatic in clinical use (Li et al., 2014). Autophagy is a well-established cell survival mechanism that promotes ATP generation by recycling metabolites when nutrients are low. Given that mTOR inhibition will lead to ULK1-dependent autophagy, it has been hypothesized that ULK1 activation and the subsequent induction of autophagy mediate some of the pro-cell survival effects that occur in response to these drugs (Jiang et al., 2015). As such, combining ULK1 inhibition with mTOR inhibition would be predicted to convert this cytostatic outcome to a cytotoxic one.

Given that autophagy can promote cell survival following a variety of cellular stresses, including in tumor cells that experience considerable ongoing metabolic stress, several labs have investigated whether autophagy inhibition, through genetic and pharmacologic means, holds utility for the treatment of cancer (Guo et al., 2013; Jiang et al., 2015; White, 2015). Recent data have suggested that lung cancers in particular may be selectively dependent on autophagy (Karsli-Uzunbas et al., 2014). However, it is clear that the role of autophagy in tumor initiation, progression, and resistance to treatment is complex and context specific. It has been suggested that at the early stages of tumor formation the enhancement of autophagic flux may be therapeutically beneficial by clearing mutant or misfolded proteins and alleviating cellular stress (White, 2015). Conversely, once a solid tumor is established and ''rewiring'' of metabolic signaling pathways has occurred in the nutrient deprived tumor core, autophagy may be upregulated to allow for cell survival under nutrient-poor conditions, posing a barrier to treatment (Kroemer, 2015). To date, most clinical efforts have focused on using the general autophagy inhibitors chloroquine (CQ) and hydroxychloroquine, either as standalone agents or in combination with other anti-cancer therapeutics such as mTOR inhibitors for the aforementioned reasons (Rangwala et al., 2014). However, the development of potent and selective autophagy inhibitors has remained largely elusive, in part because the majority of the core autophagy proteins that have been screened for small molecules lie far downstream in the pathway and are not readily druggable enzymes. As ULK1 is a potentially druggable serine/threonine kinase representing one of the first biochemical steps of autophagy, it therefore represents an attractive target for modulation by small molecules (Jiang et al., 2015). Using our identified in vivo ULK1-dependent phosphorylation events, we report here the discovery and characterization of SBI-0206965, a potent and specific small molecule ULK1 kinase inhibitor. We demonstrate the ability of this compound to suppress ULK1 downstream phosphorylation events in cells and reveal therapeutic potential for this agent in combination with mTOR inhibitors.

RESULTS

Determination of the ULK1 Kinase Consensus Phosphorylation Site

To identify additional substrates of ULK1 that may be important for the control of autophagy, we identified an optimal ULK1 phosphorylation consensus motif using arrayed degenerate peptide libraries, as we have previously performed for AMPK and AMPK-related kinases (Goodwin et al., 2014; Gwinn et al., 2008). To generate active ULK1 for these experiments, epitope-tagged ULK1 was co-expressed with its subunits FIP200 and Atg13 in HEK293T cells and peptide eluted from affinity resin. The purified ULK1 complex exhibited robust kinase activity toward a known substrate, Atg13, in a dose-responsive fashion (Figure S1A). We used the purified ULK1 complex to screen a peptide library to determine its preferred sequence surrounding the phosphorylation site (Figure 1A). The results obtained with ULK1 correlate well with recent data on the peptide substrate specificity of the budding yeast ortholog of ULK1, Atg1 (Papinski et al., 2014). Unlike other Ser/Thr kinases (Miller et al., 2008; Turk, 2008) that phosphorylate sites near charged residues or proline, ULK1 had an unusual preference for hydrophobic residues at multiple positions surrounding the phosphorylation site. In particular, ULK1 strongly preferred a Leu or Met residue at position −3, while both aliphatic and aromatic hydrophobic residues were selected in the +1 and +2 positions. In addition, ULK1 strongly prefers Ser over Thr as the phosphoacceptor residue (Figure 1B). A consensus peptide substrate (ULKtide) that incorporated residues selected at each position flanking the phosphorylation site was efficiently phosphorylated by ULK1 in vitro. Starting with this peptide, we substituted key residues in ULKtide and measured the ability of our purified ULK1 complex to utilize these mutant peptides as substrates in an in vitro kinase assay. These experiments confirmed the importance of the −3, +1, and +2 positions for maximal phosphorylation efficiency (Figure 1C).

Identification of ULK1 Substrates

A position-specific scoring matrix based on ULK1 peptide substrate specificity (Figure 1B) was used to bioinformatically search the human proteome for sites closely matching the ULK1 substrate consensus motif (Obenauer et al., 2003). We chose to focus first on those candidate substrates with highly conserved roles in autophagy, as a subset of core autophagy pathway components bears multiple ULK1 consensus sites. To define ULK1 phosphorylation sites in vivo, we took advantage of the fact that ULK1 is constitutively active when overexpressed in HEK293T cells. We therefore compared global phosphorylation events on epitope-tagged candidate targets when co-expressed with WT ULK1 or a kinase-dead (KD) version. Using mass spectrometry, we identified phosphopeptides derived from each candidate protein under these conditions. These experiments

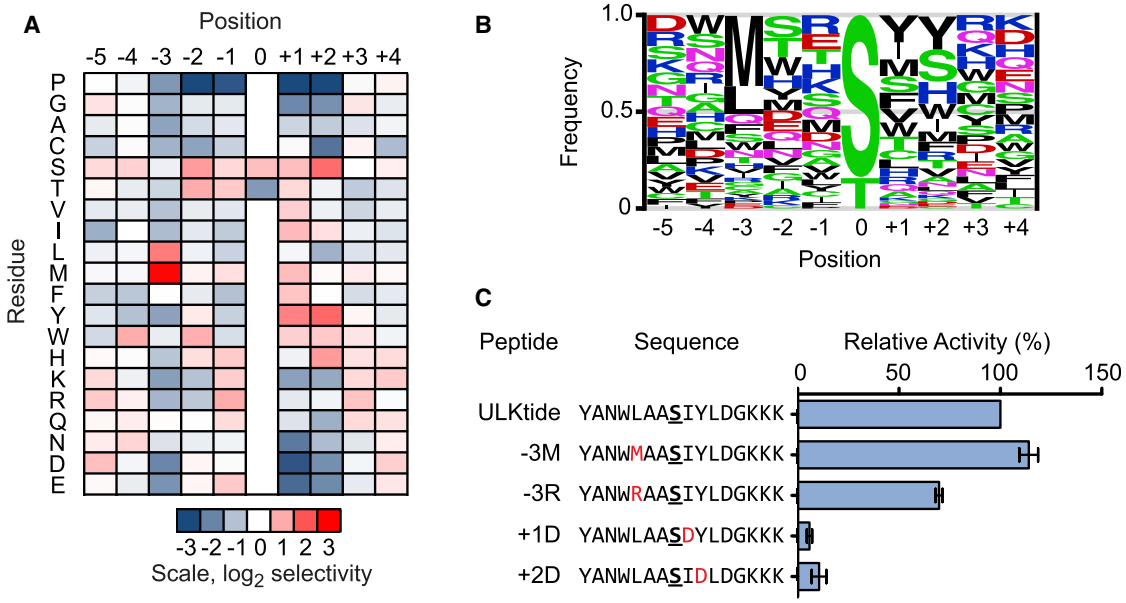

Figure 1. Determination of the Optimal ULK1 Consensus Phosphorylation Motif

(A) A positional scanning peptide library (PSPL) approach was used to define the optimal ULK1 consensus phosphorylation motif. A spatially arrayed PSPL was subjected to in vitro phosphorylation using active ULK1 and radiolabeled ATP. Each peptide contained a fixed residue at one of nine positions relative to the centrally fixed phosphoacceptor (an equal mix of Ser and Thr), with the remaining positions being equimolar mixtures of the 17 amino acids (excluding Ser, Thr, and Cys). Aliquots of each reaction were spotted onto an avidin membrane, which was washed, dried, and exposed to a phosphor-storage screen to quantify radiolabel incorporation into each peptide. The heat map was generated in Microsoft Excel using normalized and log-transformed signals corresponding to peptides with the indicated amino acid at the indicated position.

(B) Scaled sequence logo showing ULK1 sequence specificity obtained from the PSPL data. ULK1 prefers hydrophobic residues at the −3, +1, and +2 positions. The logo was generated using EnoLogos, with the height of the letter being proportional to the signal for the corresponding amino acid at the indicated position.

(C) Rates of ULK1 phosphorylation for ULKtide variants with individual amino acid substitutions are shown (normalized to unmodified ULKtide peptide). ULKtide was estimated to have a 15-μM Km. Peptide phosphorylation was assayed at a 5-μM concentration using a radiolabeled kinase assay. Incorporation of γ-^{32}P-ATP into these peptides was determined by a phosphocellulose filter-binding assay. Assays were performed in duplicate, and data show the average of three separate experiments. Data represented as the mean ± SEM.

revealed that in a subset of proteins bearing multiple ULK1 consensus sites, peptides from these candidate substrates were isolated that were highly phosphorylated in the presence of co-expressed WT but not KD ULK1. We first focused on the components of the ULK1 kinase complex itself, including FIP200, Atg13, and Atg101 (Figures 2 and S2).

Atg101 was first identified in a mass spectrometry analysis of ULK1 interactors and found to encode a highly conserved integral component of the ULK1/FIP200/Atg13 complex in mammalian cell immunoprecipitations (Hosokawa et al., 2009; Mercer et al., 2009). Atg101 binds directly to Atg13 and is critical for Atg13 stabilization and its resultant stimulation of ULK1 kinase activity. To map potential ULK1-dependent phosphorylation events in Atg101, we co-expressed Flag-tagged Atg101 with WT or KD ULK1 and performed MS/MS analysis of total peptides in the Flag-Atg101 immunoprecipitates to map total phosphorylation sites in Atg101 under the two conditions. We observed that two specific serine sites (Ser11, Ser203) within human Atg101 were stoichiometrically phosphorylated in cells co-expressing WT but not KD ULK1 (Figure 2A). Notably, these two ULK1-dependent phosphorylation sites conform well to the optimal ULK1 substrate motif, in particular having hydrophobic residues at the −3 and +1 positions, which suggests that they may be direct ULK1 substrates in vivo. To further explore ULK1 phosphorylation of Atg101 in cells, we examined the migration pattern of Atg101 during SDS-PAGE in gels containing the Phos-Tag reagent, a phosphate binding dinuclear metal complex that specifically retards the mobility of phosphoproteins (Kinoshita et al., 2006). Comparing the mobility pattern of Atg101 on a Phos-Tag gel revealed a robust mobility change suggestive of phosphorylation (Figure 2B) when co-overexpressed in HEK293T cells with WT ULK1. Mutation of Atg101 Ser11 abolished much of the mobility change, and this was further enhanced by additional mutation of Ser203 and nearby sites, which corroborated their identification as potential ULK1-dependent sites by mass spectrometry. We next performed a similar analysis of FIP200 and Atg13 phosphorylation events, and we discovered multiple serine sites in FIP200 and Atg13 bearing the ULK1 substrate consensus whose phosphorylation was induced by overexpressed WT ULK1 in cells (Figures S2A and S2B).

Next, we examined components of the Beclin1/Vps34 complex, which lies directly downstream of the ULK1 complex in autophagy initiation (Kim and Guan, 2015). Similar to Atg101, mass spectrometry identified sites of phosphorylation in Beclin1 induced by co-expression of WT but not KD ULK1 in HEK293T cells, and those sites most extensively phosphorylated in this

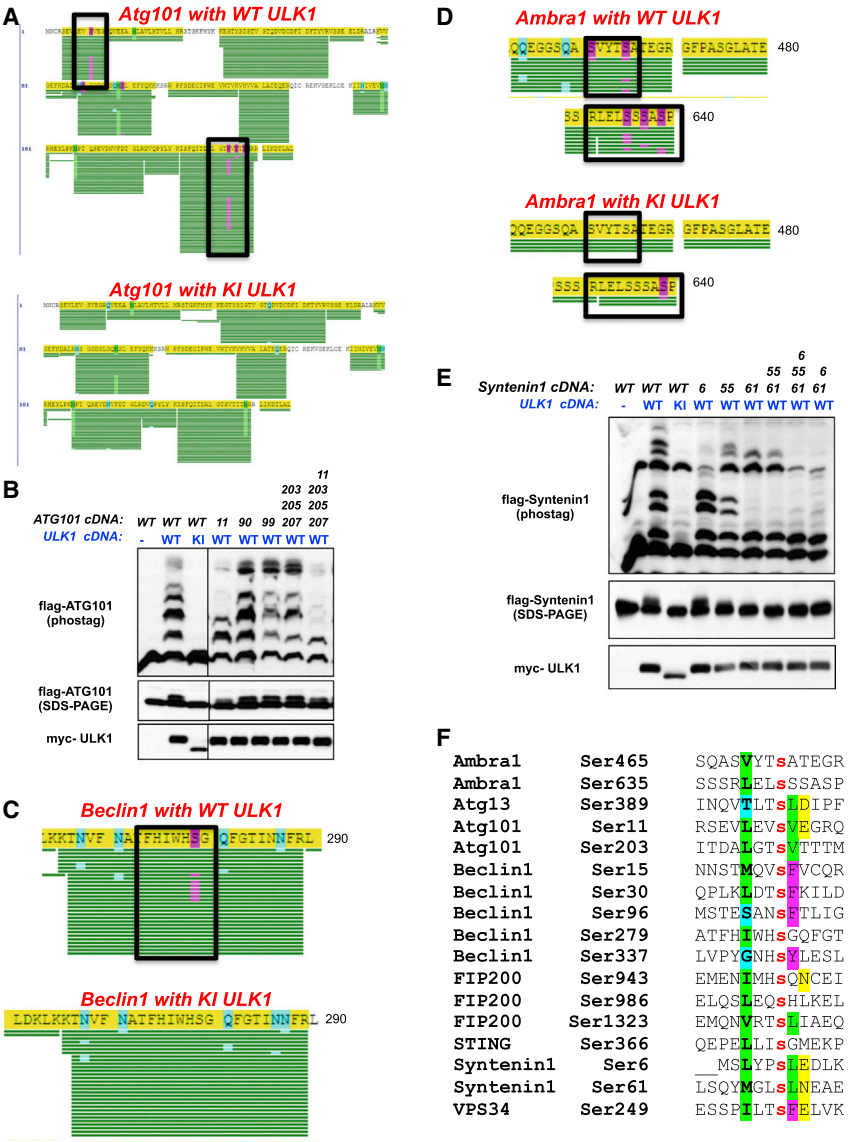

Figure 2. Identification of Novel ULK1-Dependent Phosphorylation Sites In Vivo

(A) Myc-tagged WT ULK1 (WT ULK1; top) or Myc-tagged kinase-inactive ULK1 (KI ULK1; bottom) was transfected into HEK293T cells along with WT Flag-tagged Atg101 (Flag-Atg101) and immunoprecipitated with M2 agarose. The immunoprecipitate was run out on an SDS-PAGE gel and stained with coomassie, and the band corresponding to Flag-Atg101 was cut out, isolated, and subjected to tryptic digest and LC/MS/MS analysis. The phosphorylated sites that conform to the optimal ULK1 phosphorylation motif that were identified by this analysis are boxed. Green bars indicate peptide coverage, and purple highlights indicate phosphorylation events.

(B) WT ULK1 or KI ULK1 was transfected into HEK293T cells along with Flag-Atg101 or Flag-Atg101 serine-to-alanine point mutants. The specific mutants used in this analysis are indicated by the position(s) of the substituted amino acid (top). Cellular lysates were isolated 24-hr post-transfection, run out on an SDS-PAGE gel containing the Phos-Tag reagent (middle) or a standard SDS-PAGE gel lacking the Phos-Tag reagent (bottom), and transferred to PVDF membranes, which were subsequently immunoblotted with the indicated antibodies.

(C) Same as (A) except using WT Flag-tagged Beclin1 as a substrate.

(D) Same as (A) except using WT Flag-tagged Ambra1 as a substrate.

(E) Same as (B) except using WT Flag-tagged Syntenin-1 (Flag-Syntenin-1) or Flag-tagged Syntenin-1 serine-to-alanine point mutants. The specific mutants used in this analysis are indicated by the position(s) of the substituted amino acid (top). Cellular lysates were isolated 24-hr post-transfection, run out on an SDS-PAGE gel containing the Phos-Tag reagent (middle) or a standard SDS-PAGE gel lacking the Phos-Tag reagent (bottom), and transferred to PVDF membranes, which were subsequently immunoblotted with the indicated antibodies.

(F) Alignment of all novel ULK1 phosphorylation sites identified in this analysis, alongside the STING phosphorylation site, which was previously reported as a ULK1 site (Konno et al., 2013). Phosphorylation sites that contain residues conforming to the optimal ULK1 phosphorylation motif at the −3 (green), +1 (green), and +2 (yellow) positions are highlighted.

context matched the ULK1 optimal substrate sequence, suggesting that Beclin1 may also be a direct ULK1 substrate (Figure 2C). Further analysis identified additional serine residues in Beclin1 that conform to the optimal ULK1 phosphorylation motif that were not observed by mass spectrometry analysis, and some of these contributed to Beclin1 mobility changes on Phos-Tag gels (Figure S2C). One of these sites, Ser15, was recently identified as a site of ULK1 phosphorylation and was reported to play a conserved role in autophagy induction (Russell et al., 2013). We found that mutation of at least three of these serine residues (Ser15, Ser30, Ser337) was required to prevent the observed mobility shift on Phos-Tag gels (Figure S2C). Examination of another component of the Beclin1 complex, Ambra1, also revealed multiple ULK1-dependent phosphorylation events in cells, suggesting that many components of the Beclin/Vps34 complex may be targeted by ULK1 (Figure 2D). Finally, we examined a known ULK1 interacting protein, Syntenin-1, which was also reported as an ULK1 substrate (Rajesh et al., 2011). Here, we found that the previously reported in vitro phosphorylation site, Ser6, along with a second site, Ser61, are jointly responsible for altered mobility of Syntenin-1 in the presence of ULK1 in vivo (Figure 2E). Collectively, the majority of the candidate ULK1 phosphorylation sites we identified across these substrates contain hydrophobic residues in the −3 position (Figure 2F), consistent with our identified optimal ULK1 substrate sequence (Figure 1B) and with another site recently reported in another ULK1 substrate, STING (Konno et al., 2013). In contrast with the preferred peptide sequence, hydrophobic residues

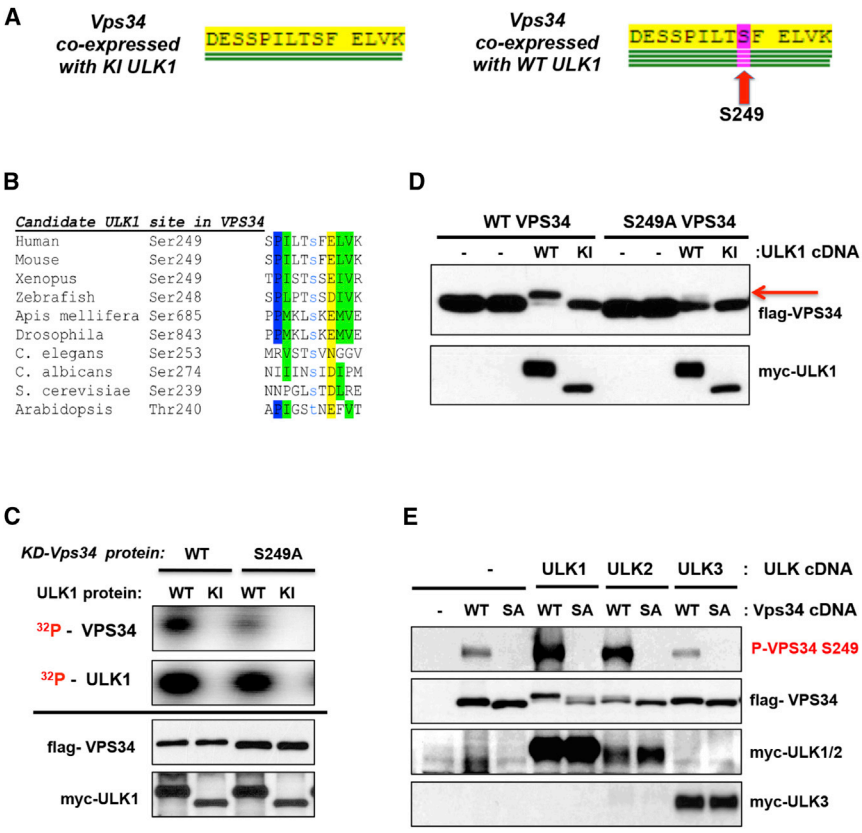

Figure 3. Vps34 Ser249 Is a Novel ULK1 Phosphorylation Site In Vivo

(A) Either Myc-tagged WT ULK1 (WT ULK1; right) or Myc-tagged kinase-inactive ULK1 (KI ULK1; left) was transfected into HEK293T cells along with WT Flag-tagged Vps34 (WT Vps34) and immunoprecipitated with M2 agarose. The immunoprecipitate was run out on an SDS-PAGE gel and stained with coomassie, and the band corresponding to WT Vps34 was cut out, isolated, and subjected to tryptic digest and LC/MS/MS analysis. Green bars indicate peptide coverage, and purple highlights indicate phosphorylation events. Arrow indicates serine 249.

(B) Clustal alignment of Vps34 serine 249 across species shows that it is conserved throughout evolution and conforms to the optimal ULK1 phosphorylation motif.

(C) An in vitro kinase assay was performed using Flag-tagged WT Vps34 (Vps34 WT) or a Flag-tagged serine-to-alanine point mutant Vps34 (Vps34 S249A) as substrates for either WT ULK1 or KI ULK1. The in vitro kinase assay was performed in the presence of radiolabeled γ-^{32}P-ATP (top). Vps34 WT, Vps34 S249A, WT ULK1, and KI ULK1 were produced in HEK293T cells (bottom).

(D) Vps34 WT or Vps34 S249A and WT ULK1 or KI ULK1 were transfected into HEK293T cells. Cellular lysates were isolated 24-hr post-transfection, run out on an SDS-PAGE gel, and transferred to PVDF membranes, which were subsequently probed with the indicated antibodies. Arrow indicates a mobility shift representative of phosphorylation that only occurs with the Vps34 WT and WT ULK1 combination.

(E) HEK293T cells were transfected with Vps34 WT or Vps34 S249A and WT ULK1, WT Myc-tagged ULK2 (ULK2), or WT Myc-tagged ULK3 (ULK3). Cellular lysates were isolated 24-hr post-transfection and immunoblotted with the indicated antibodies.

were not overrepresented at the +2 position, possibly because short sequence motifs bearing three hydrophobic residues in close proximity might be inaccessible to phosphorylation by kinases.

In contrast to the majority of the substrates we examined that contained between two to four ULK1-dependent phosphorylation sites, one protein, the lipid kinase Vps34, apparently contained only a single ULK1 phosphorylation site (Figure 2F). The highly conserved Ser249 of Vps34 was stoichiometrically phosphorylated in HEK293T cells when co-expressed with WT but not KD ULK1 (Figures 3A and 3B). Mutation of Ser249 alone was sufficient to abolish phosphorylation of Vps34 by ULK1 in vitro (Figure 3C) and prevented a ULK1-induced mobility shift on a standard SDS-PAGE gel upon co-expression in cells (Figure 3D).

We explored the potential function of Vps34 phosphorylation by ULK1 by introducing non-phosphorylatable (Ser249Ala) or phospho-mimetic (Ser249Asp) mutants into conditional Vps34-floxed murine embryonic fibroblasts (MEFs) (Jaber et al., 2012). After first corroborating the requirement of Vps34 for proper autophagy and ultimate cell viability (Figure S3A, data not shown), we tested the effects of these mutants in five assays of Vps34 function in autophagy. However, Ser249 in Vps34 was not required under the conditions we examined (Figures S3B–S3E). Given that ULK1 appears to phosphorylate multiple sites in Beclin1 and Ambra1 at the same time that it is phosphorylating Ser249 of Vps34, the data suggest that the sum effects of ULK1 on the different Beclin1/Vps34 subcomplexes is a highly regulated series of events requiring further study.

We next developed a phospho-specific antibody to Vps34 Ser249, whose signal was increased when ULK1 or ULK2, but not ULK3, was co-expressed with WT Vps34 but not a Ser249Ala Vps34 mutant in HEK293T cells (Figure 3E).

Identification and Characterization of a Small Molecule Inhibitor of ULK1

To further examine how ULK1 regulates autophagy, we sought to identify small molecule inhibitors of the kinase. Starting with a focal adhesion kinase (FAK) inhibitor that showed potent cross-reactivity toward ULK1, we used a target-based reverse pharmacology approach to screen a focused library of pyrimidine analogs to identify small molecule ULK1 inhibitors. We performed in cellulo screening of the most promising 100 analogs from the in vitro kinase screening, testing their dose-dependent ability to inhibit the phosphorylation of Vps34 Ser249 by co-expressed ULK1 in HEK293T cells. Structure-activity relationship (SAR) data were used to drive medicinal

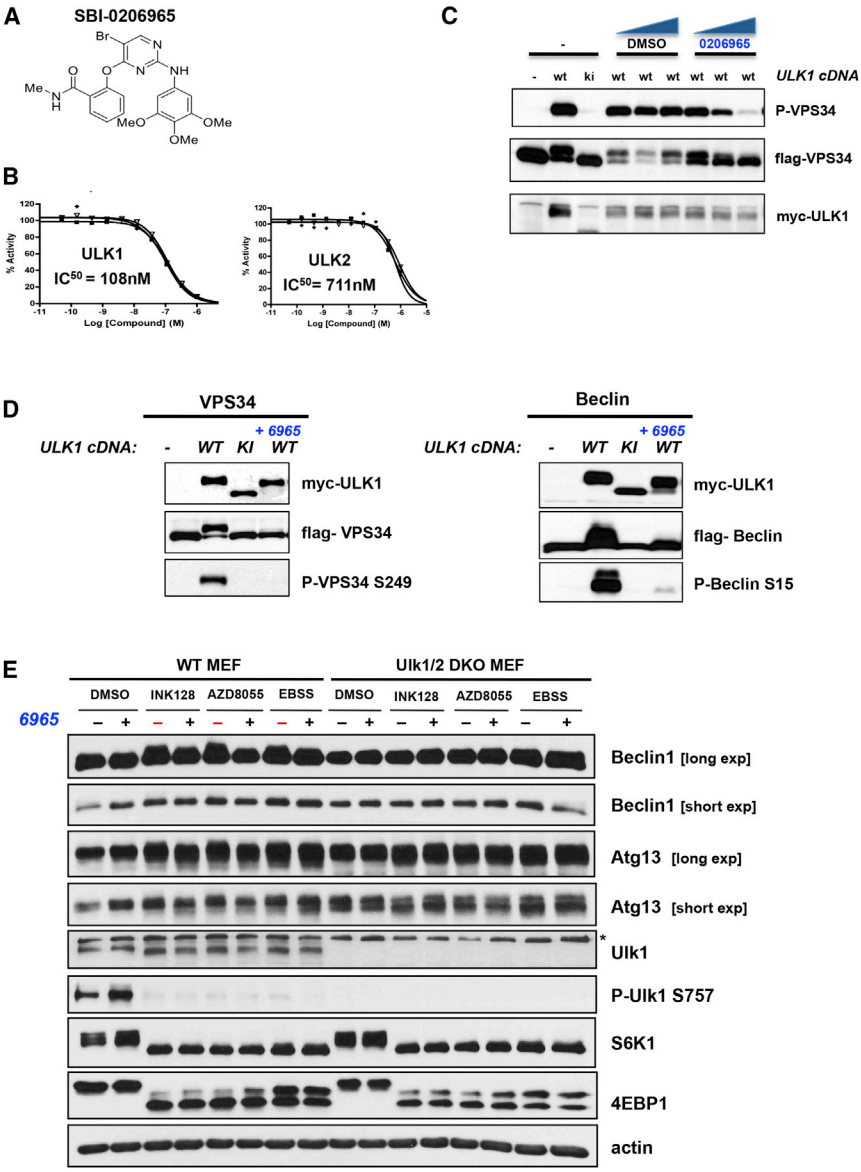

Figure 4. In Cellulo Screen Identifies SBI-0206965 as a Potent ULK1 Kinase Inhibitor against Its Downstream Substrate Phosphorylation Sites

(A) Chemical structure of SBI-0206965 ("6965"), the lead ULK1 competitive kinase inhibitor.

(B) The IC_{50} value for 6965 against WT ULK1 and ULK2 was determined using an in vitro kinase assay. WT ULK1 (left) and WT ULK2 (right) were assayed using 10-μM MBP in the presence of 30-μM radiolabeled γ-^{32}P-ATP. 6965 was tested in triplicate in a ten-dose IC_{50} mode with 3-fold serial dilution and a starting dose of 1 μM.

(C) Human embryonic kidney cells (HEK293T) were transfected with WT or kinase inactive (KI) Myc-tagged ULK1 and WT Flag-tagged Vps34 (WT Vps34). At 24-hr post-transfection, cells were treated with a panel of putative ULK1 competitive inhibitors in a dose-response manner (1, 10, 50 μM). Cellular lysates were isolated after 1 hr of treatment and immunoblotted with the indicated antibodies. Representative results for SBI-0206965 are shown.

(D) HEK293T cells were transfected with WT or KI ULK1 and WT Vps34 (left) or WT Flag-tagged Beclin1 (WT Beclin1; right). At 24-hr post-transfection, cells were treated with 6965 (10 μM) or DMSO. Cellular lysates were isolated after 1 hr of treatment and immunoblotted with the indicated antibodies.

(E) WT or *Ulk1/Ulk2* double knockout mouse embryonic fibroblasts (MEFs) (Cheong et al., 2011) were treated with fresh media (Dulbecco's modified Eagle medium [DMEM] containing 10% FBS) containing 1-μM INK128, 1-μM AZD8055, or DMSO or with starvation media (EBSS) in the presence or absence of 10 μM 6965. Cellular lysates were isolated after 1 hr of treatment and immunoblotted with the indicated antibodies. Asterisk denotes non-specific band.

chemistry efforts that led to the ULK1 inhibitor tool compound SBI-0206965 (Figure 4A). Dose-response analysis of SBI-0206965 revealed an in vitro IC_{50} of 108 nM for ULK1 kinase activity and 711 nM for the highly related kinase ULK2 (Figure 4B). We found SBI-0206965 (hereafter referred to as "6965") inhibited Ser249 phosphorylation of overexpressed Vps34 when used at ~5 μM (Figure 4C). To ensure that 6965 was not specifically selective toward phosphorylation of Vps34 Ser249, we examined its ability to inhibit the phosphorylation of other ULK1 substrates we had identified. After validating a commercial antibody that could recognize a ULK1 phosphorylation site in Beclin1 (Ser15) when Beclin1 is overexpressed (Figure S4A), we found that 6965 inhibited Beclin1 Ser15 and Vps34 Ser249 phosphorylation to comparable extents in HEK293T cells (Figure 4D). Furthermore, 6965 treatment collapsed the bandshift that Syntenin-1 and Atg13 undergo when co-expressed with WT ULK1 (Figures S4B and S4C). Unfortunately, none of these existing phospho-specific antibodies against the ULK1 sites in Beclin1 or Vps34 is sensitive enough to recognize the endogenous proteins in a total cell lysate.

We next examined whether 6965 would inhibit endogenous ULK1 activity. To activate endogenous ULK1, we treated MEFs with either amino acid starvation media (Earle's balanced salt solution [EBSS]) or the mTOR ATP-competitive inhibitors INK128 or AZD8055 (Chresta et al., 2010; Hsieh et al., 2012). In WT MEFs, we observed a mobility shift in endogenous Beclin1 and Atg13 in response to EBSS starvation media or the mTOR catalytic inhibitors, which was abolished in *Ulk1/2*-deficient MEFs (Figure 4E). The EBSS and mTOR-inhibitor induced mobility shift in Beclin1 and Atg13 was inhibited by 6965 co-treatment in WT MEFs (Figure 4E). Notably, neither Beclin1 nor Atg13 underwent a mobility shift upon treatment with either EBSS or the mTOR catalytic inhibitors in *Ulk1/2*-deficient MEFs, and no further decrease in their basal mobility was observed with 6965 co-treatment. We

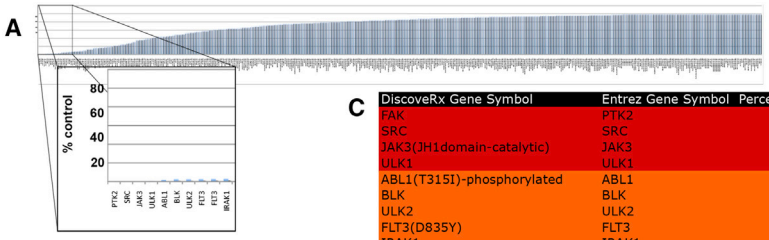

C

DiscoveRx Gene Symbol	Entrez Gene Symbol	Percent Control
FAK	PTK2	0.2
SRC	SRC	0.25
JAK3(JH1domain-catalytic)	JAK3	0.4
ULK1	ULK1	0.8
ABL1(T315I)-phosphorylated	ABL1	2.1
BLK	BLK	2.6
ULK2	ULK2	2.6
FLT3(D835Y)	FLT3	2.8
IRAK1	IRAK1	3.2
ERK2	MAPK1	3.4

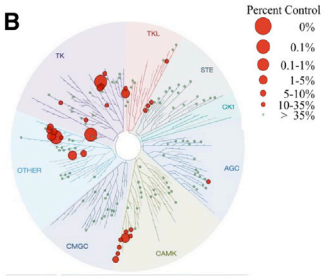

D

KINASE:	Relative IC50	Fold vs ULK1
FAK	4.122E-08	0.4
c-Src	5.674E-07	5.7
JAK3	5.954E-07	6.0
ULK1	1.08E-07	1.0
ABL1 (T315I)	2.352E-06	23.5
BLK	2.128E-06	21.3
ULK2	7.110E-07	6.6
FLT3	7.932E-08	0.8
IRAK1	9.313E-07	9.3
ERK2/MAPK1	8.338E-06	83.4

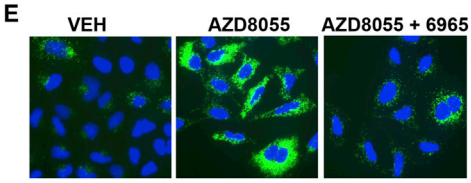

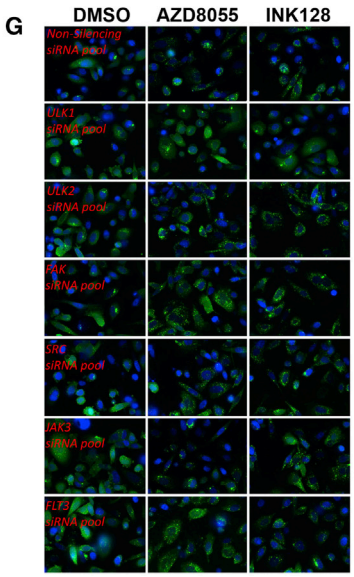

F

siRNA pools	DMSO		1uM AZD 8055		1uM INK128	
GeneSymbol	AVG	STD	AVG	STD	AVG	STD
siRNA Control	9.8	0.1	20.2	0.7	19.9	0.8
ULK1	6.9	0.4	8.5	0.3	8.4	1.9
ULK2	11.7	2.4	20.0	1.1	21.1	0.6
PTK2 (FAK)	9.5	0.1	20.0	0.4	20.7	1.5
SRC	11.6	0.2	22.8	0.0	22.6	1.0
c-SRC	12.1	0.2	23.5	0.1	21.6	1.1
JAK3	9.8	0.7	18.1	0.5	19.1	1.2
JAK2	11.8	0.5	20.3	0.9	17.9	0.8
ABL1	8.1	0.1	18.9	0.5	16.1	0.6
BLK	10.1	0.6	18.3	0.5	20.0	0.9
FLT3	9.7	0.1	15.3	0.0	17.2	1.5
IRAK1	12.5	1.3	16.9	2.3	17.6	0.8
AURKA (AuroraA)	13.1	0.8	16.2	3.7	17.1	0.9
AURKC (AuroraC)	9.8	1.3	18.2	0.9	20.8	1.9
SNARK (NUAK2)	13.8	0.7	16.4	1.2	14.8	0.1
TYK2	8.8	1.3	16.5	3.2	13.0	1.9
PAK1	9.5	0.8	16.6	0.1	17.8	1.0
MAPK1 (ERK2)	9.5	0.3	16.3	0.1	18.7	1.1
PLK4	9.6	0.1	19.9	1.6	19.8	2.8

puncta per cell

Figure 5. SBI-0206965 Is a Highly Selective Kinase Inhibitor

(A) The kinase selectivity profile for SBI-0206965 was determined using the DiscoveRx KINOMEscan profiling service (http://www.discoverx.com/). Briefly, 6965 was screened at a 1-μM dose for its ability to impair binding of a panel of 456 kinases to substrate in an in vitro binding assay. Scores for the primary screen hits are reported as a percent of the DMSO control (% Control). Lower scores reflect stronger inhibitory effects of 6965 on the target kinase.

(B) A TREEspot interaction map (http://www.discoverx.com/tools-resources/interaction-maps) was generated to visually represent the selectivity profile for 6965 against the panel of kinases tested in 5A. Kinases whose binding was inhibited by 6965 are marked with red circles, with larger circles indicating stronger inhibitory effects. Kinases tested in this analysis are arrayed according to their phylogenetic groupings in the human kinome.

(C) The list of the kinases whose binding was found to be inhibited by 6965 to less than 4% of the DMSO-negative control in the screen described in 5A. Kinases whose binding was inhibited to less than 1% of the DMSO-negative control are highlighted in red.

(D) In vitro kinase assays were performed for the kinases highlighted in 5C. These assays were performed in the presence of 6965 in a dose-response manner to identify the IC_{50} value for 6965 for each of these individual kinases. Kinases whose IC_{50} value was less than 1-fold difference than ULK1 are highlighted in yellow. Of the remaining kinases, those kinases whose IC_{50} value was less than what was identified for ULK2 are highlighted in brown. In vitro kinase assays performed by Reaction Biology (http://www.reactionbiology.com/).

(E) Immunoflourescence imaging of A549 cells treated in the presence or absence of 5 μM 6965 for 2 hr followed by 4 μM of the mTOR catalytic inhibitor AZD8055 for 24 hr. Autophagic vacuoles were detected using the Cyto-ID autophagy detection kit (Chan et al., 2012) and are visualized in green, while cell nuclei were counterstained by DAPI and are visualized in blue.

(F) PC3 human prostate cells that stably express a construct encoding LC3 fused to green fluorescent protein (GFP-LC3) were transfected with siRNAs against the top 18 kinases whose binding was shown to be inhibited by 6965 (Figure 5A). At 48 hr after RNAi transfection, the cells were treated with 1 μM of the catalytic mTOR inhibitors AZD8055 or INK128 for 4 hr and assessed for the presence of GFP-LC3 puncta (see Experimental Procedures). The average number of GFP-LC3 puncta and SD for each siRNA and drug treatment are shown. Control immunoblots demonstrating siRNA efficiency are shown in Figure S5E. SRC, c-Src; c-Src kinase, CSK.

(G) Representative immunofluorescence images for the data shown in 5F. GFP-LC3 puncta are visualized in green and cell nuclei, which were counterstained with DAPI, are visualized in blue.

hypothesize that the mobility shifts observed in endogenous Beclin1 and Atg13 induced by mTOR inhibitors and starvation media reflect phosphorylation of endogenous Beclin1/Atg13 by endogenous ULK1/2 as they only occur in WT but not *Ulk1/2*-deficient MEFs.

SBI-0206965 Is a Highly Selective Kinase Inhibitor

We next examined the specificity of 6965 using the DiscoveRx KINOMEscan panel of 456 purified human kinases in a competition-binding assay (Fabian et al., 2005; Karaman et al., 2008). By this analysis, 6965 was very selective, only inhibiting 10 out of 456 kinases >95% when tested at 10 μM (Figures 5A and 5B). The S(35) selectivity index of 6965 was 0.123, as measured by the percentage of the kinome inhibited below 35% of the control at this concentration (Figures S5A and S5B) (S[35] = [number of kinases with %Ctrl < 35]/[number of kinases tested]). This makes the selectivity profile of 6965 comparable to several kinase inhibitors currently used in clinical oncology, including Imatinib and Lapatinib (Figure S5B). Notably, by this assay, all the kinases bound by SBI-0206965 with an affinity comparable to ULK1

(FAK, Src, Abl, and Jak3) were tyrosine kinases (Figure 5C). Moreover, the only known functional ULK1 homolog in mammals, ULK2, was inhibited almost as well as ULK1 in this assay (Figure 5C), consistent with measurements obtained from in vitro kinase assays (Figure 4B).

We subsequently measured the selectivity of SBI-0206965 against its top binding kinases using radiolabel kinase assays in vitro at varying inhibitor concentrations. Here, we tested the ten kinases whose binding was most suppressed by 6965 by the DiscoverRx ATP binding assay (from Figure 5C). Of these kinases, only FAK and FLT3 showed an IC_{50} comparable to ULK1 when measured by an in vitro kinase assay (Figure 5D), and 6965 inhibited Src, Jak3, and ULK2 5- to 10-fold less potently than ULK1 and FAK. Consistent with its efficacy of FAK inhibition in vitro, we found that at 10 μM, 6965 reduced endogenous FAK signaling in HEK293T cells (as judged by FAK and Paxillin phosphorylation) to an extent comparable to its inhibition of ULK1 signaling, albeit when ULK1 was overexpressed (Figure S5C). To examine the selectivity of 6965 more rigorously, we examined its impact on endogenous ULK1 and FAK signaling, as well as a number of other critical growth pathways, in WT MEFs that were starved or treated with mTOR inhibitors to endogenously activate ULK1 (Figures 4E and S5D). Notably, in MEFs, 6965 did not impair endogenous FAK, AMPK, mTOR, Akt, or Erk signaling at 10 μM, a dose at which it is capable of preventing a mobility shift in Atg13 that occurs in response to mTOR inhibition (Figure 4E and S5D). The suppression of endogenous ULK1 signaling was also monitored by a very recently developed phospho-specific antibody to one of the ULK1 sites in Atg13 (Ser318, which is Ser355 in human Atg13 isoform1) (Figure S5D). In fact, at 10 μM, 6965 only modestly reduced FAK and Src signaling (as judged by FAK and Paxillin phosphorylation) and increased both AMPK and Erk-dependent signaling with increasing doses (Figure S5D). Thus, 6965 appears quite selective for ULK1 in vitro and in vivo, with a secondary selectivity toward FAK.

SBI-0206965 Suppresses Autophagy Induced by mTOR Inhibition, and This Is Phenocopied by ULK1 siRNA

To test the ability of 6965 to block autophagy and cell survival, initial studies were performed in A549 lung cancer cells, which are highly sensitive to mTOR inhibition (Sun et al., 2005). We observed that the catalytic ATP-competitive mTOR kinase inhibitor AZD8055 induced robust autophagy as visualized by accumulation of the Cyto-ID autophagy dye (Chan et al., 2012), and this effect was strongly suppressed by treatment with 5-μM 6965 (Figure 5E). Next, we genetically assessed the requirement for ULK1 versus other kinases inhibited by 6965 to induce autophagy after pharmacological mTOR inhibition. A robust high-throughput microscopy method for quantifying GFP-LC3 puncta was established using a PC3 prostate-cancer cell line stably expressing a GFP-LC3 construct (Degtyarev et al., 2008). Using this assay, we performed a focused RNAi analysis of the top 20 kinases identified in the DiscovRx screen as best binding to 6965. Quantitative measurement on wells of cells transfected with control siRNAs revealed a consistent 2-fold induction in GFP-LC3 puncta formation after treatment with either of the mTOR catalytic inhibitors INK128 or AZD8055 (Figures 5F and 5G). Strikingly, of the 18 kinases tested, only one kinase siRNA, ULK1, nearly fully abolished the LC3 puncta induced by the mTOR inhibitors (Figures 5F and S5E). The ability of ULK1 siRNA to nearly fully ablate the autophagic response induced by mTOR inhibition suggests that, in this cell line at least, ULK1 is essential for stimulating autophagy in response to mTOR suppression.

SBI-0206965 Prevents ULK1-Dependent Cell Survival following Nutrient Deprivation

A well-established function of autophagy is to promote cell survival under conditions of nutrient deprivation. For example, ATG5-deficient immortal, nontumorigenic baby mouse kidney epithelial cells display no growth defects when cultured under normal media conditions; however, when such cells are placed into starvation media, they undergo apoptosis at a greatly accelerated rate compared with controls (Guo et al., 2011). Similarly, we previously demonstrated that RNAi against ULK1 and ULK2 phenocopied RNAi against ATG5 with regards to the loss of cell viability under nutrient-deprived conditions (Egan et al., 2011b). To examine whether our small molecule ULK1 inhibitor would similarly affect cell survival under nutrient-deprived conditions, we treated MEFs with 6965 in the context of normal media, amino acid-deprived media, or glucose-deprived media. After 18 hr of amino acid deprivation, 15% of the vehicle-treated MEFs were positive for both 7-AAD and AnnexinV, indicative of end-stage apoptosis (Figure 6A) versus 42% of the 6965-treated cells. Similar effects were also seen in glucose-deprived MEFs, where 6965 also promoted enhanced cell death (Figure S6A). An immunoblot time course analysis of amino-acid-starved cells revealed that active cleaved caspase-3 and the cleavage of its target PARP was only robustly observed in starved, 6965 co-treated cells (Figure 6B). Interestingly, the immunoblot analysis revealed that 6965 treatment induced the loss of ULK1 and Atg13 protein, but only in nutrient-deprived and not nutrient-replete conditions. Perhaps only in this context when ULK1 is activated does the direct binding of 6965 stimulate ULK1 turnover. We also directly compared 6965 to CQ, a lysosomotropic agent that acts as a general autophagy inhibitor (Kroemer, 2015), in their ability to drive apoptosis under starvation conditions. While both 6965 and CQ induced cell death only under starvation conditions, it was notable that 10-μM 6965 was more effective than 20-μM CQ at rapidly inducing apoptosis in this context (Figure S6B). Control immunoblotting revealed that 20-μM CQ was effective at blocking autophagic flux, preventing the turnover of the Atg8 family member LC3 as well as the autophagy cargo receptor p62/SQSTM1 (Figures 6B and S6C). The degradation of both ULK1 and Atg13 was again specifically observed under starvation conditions in cells treated with 6965 (Figure S6C). Of note, administration of CQ or bafilomycin A1, but not the proteasome inhibitor MG132, abrogated the degradation of both ULK1 and Atg13, indicating that their own turnover is lysosomal in nature (Figure S6D).

Beyond the general role of autophagy that occurs in many cell types as a response mechanism to nutrient deprivation, there has also been considerable interest in the role of autophagy as a survival mechanism for tumor cells faced with nutrient limitations due to poor vascularization as well as metabolic stress

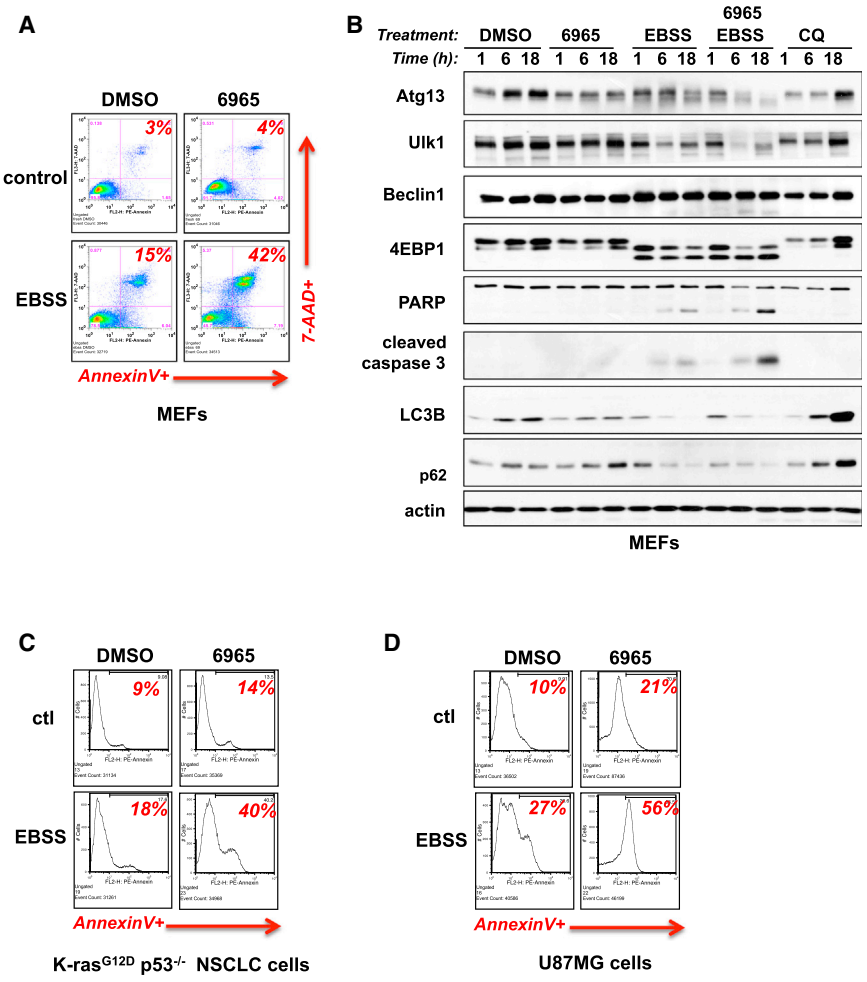

Figure 6. SBI-0206965 Synergizes with Starvation and mTOR Inhibition to Induce an Enhanced Apoptotic Response

(A) WT MEFs were treated with fresh media (DMEM containing 10% FBS) or starvation media (EBSS) and 10-μM 6965 or DMSO for 18 hr. Cells were collected, stained with 7-AAD and PE-AnnexinV, and quantified for apoptosis by fluorescence-activated cell sorting (FACS) analysis. Red numbers indicate the percentage of 7-AAD/PE-AnnexinV double-positive cells, representative of end-stage apoptosis and death.

(B) Western analysis of WT MEFs treated as in (A) for 1, 6, and 18 hr. Cellular lysates were immunoblotted with the indicated antibodies. CQ at 20 μM serves as a positive control for autophagy inhibition.

(C) Same as (A) except using a lung cancer cell line derived from a genetically engineered mouse model of lung cancer driven by mutant Kras and deletion of p53. Red numbers indicate the percentage of AnnexinV-positive cells.

(D) Same as (A) except using the human glioblastoma cell line U87MG. Red numbers indicate the percentage of AnnexinV-positive cells.

resulting from chemotherapies or targeted therapeutics (White, 2015). We examined whether 6965 would selectively promote apoptosis under conditions in which autophagy is actively engaged in tumor cells similar to what we observed in MEFs. Indeed, 6965 promoted apoptosis (AnnexinV+ cells) particularly in the nutrient-starved state in human U87MG glioblastoma cells and in murine lung carcinoma cells derived from a genetically engineered mouse model of lung cancer driven by mutant Kras and loss of p53 (Figures 6C and 6D). Notably, these murine lung cancer cells have been previously shown to be particularly dependent on autophagy (Guo et al., 2013).

The Small Molecule ULK1 Inhibitor SBI-0206965 Converts the Cytostatic Response to Catalytic mTOR Inhibitors into a Cytotoxic Response

Given that mTOR inhibition induces ULK1 activation (Figures 4E and S5C) and ULK1 siRNA or 6965 suppresses autophagy induced by mTOR inhibitors (Figures 5E–5G), we examined whether 6965 would reduce cell survival in the face of mTOR inhibition. A549 cells were treated with a constant dose of AZD8055 (1 μM), which induces cytostatic growth arrest, and escalating doses of 6965. At a 5-μM dose, 6965 triggered apoptosis in 23% of cells when combined with AZD8055 versus 10% of cells in the absence of AZD8055 and 7% of cells treated with AZD8055 alone (Figure 7A). The induction of AnnexinV+ apoptotic cells was heightened at 10-μM dosing of 6965. As observed in MEFs with nutrient deprivation combined with 6965, immunoblot analysis revealed that only the combination of 6965 with mTOR inhibitors triggered caspase activation in A549 cells, paralleling the FACS analysis of cell death (Figure S7A). Moreover, degradation of total ULK1 and Atg13 was observed as before (Figures 6B and S6C), only in the presence of the autophagy activating stimulus (AZD8055) and 6965 (Figure S7A).

To examine whether 6965 would broadly synergize with other mTOR inhibitors, we examined the ability of rapamycin and a second mTOR catalytic inhibitor, INK128 (MLN0128), to synergize with 6965 (Figure 7B). Similar to AZD8055, both rapamycin and INK128 exhibited a mild apoptotic response on their own in A549 cells but significantly enhanced this apoptotic response when combined with 6965 (Figure 7B). Notably, the extent of AnnexinV+ apoptotic cells induced by the three different mTOR inhibitors was mirrored by the proportion of Atg13 protein loss and the extent to which Beclin1 mobility was impaired (Figure 7C). This also appeared to reflect the potency of mTOR inhibition, as assessed by 4EBP1 mobility shift and loss of the direct mTOR phosphorylation of ULK1 on Ser757 (Figure 7C). A model for the selectivity of different mTOR substrates for inhibition by rapamycin or catalytic mTOR inhibitors proposed that substrate quality may dictate how easily a substrate phosphorylation site is blocked by mTOR inhibition (Kang et al., 2013). From this analysis, ULK1 was identified an excellent mTOR substrate in vitro, similar to 4EBP1 and required full mTOR catalytic inhibition to

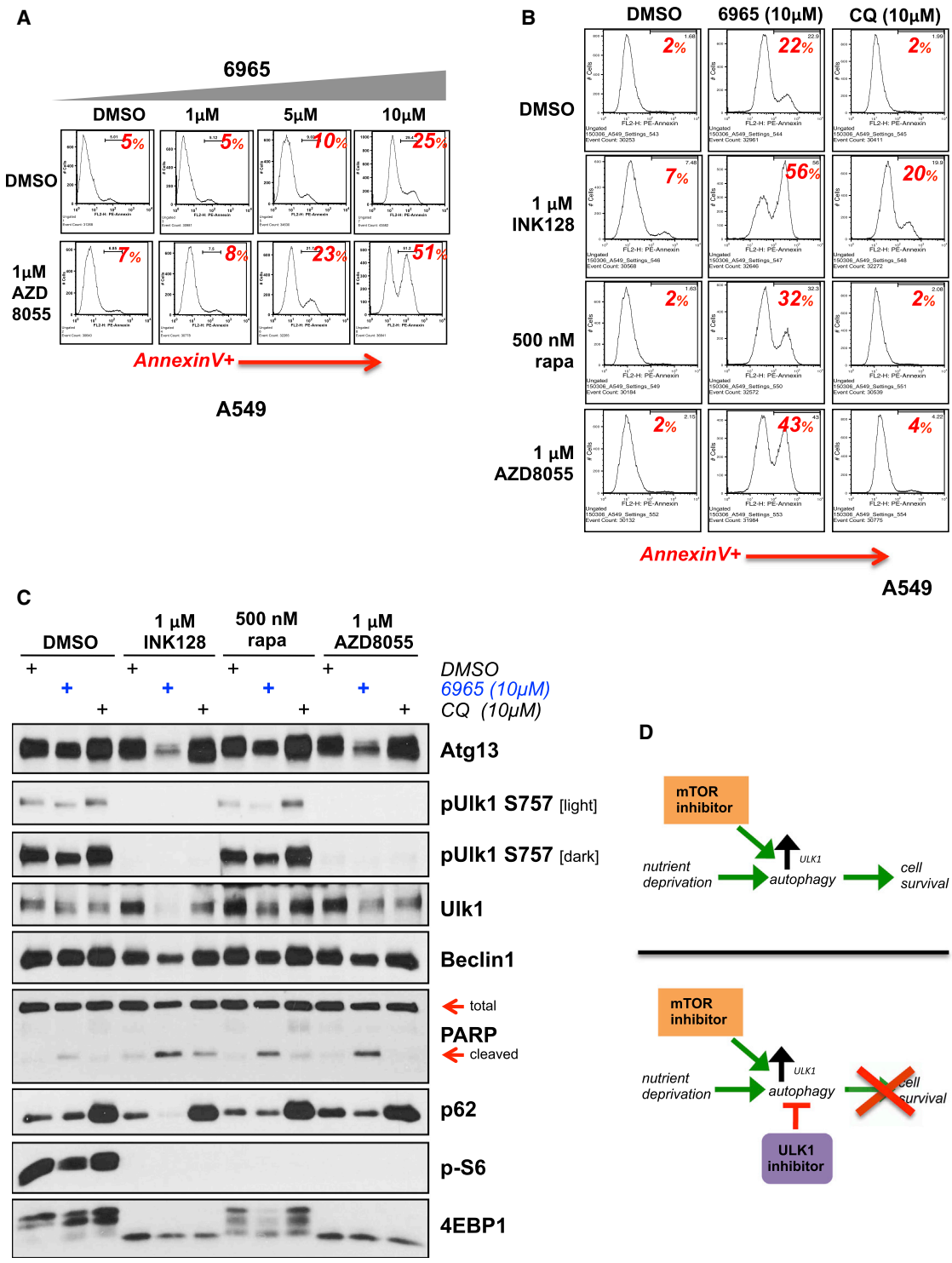

Figure 7. SBI-0206965 Converts the Cytostatic Effects of Three Different mTOR Inhibitors into a Cytotoxic Apoptotic Response in Lung Cancer Cells

(A) A549 human lung cancer cells were treated with the catalytic mTOR inhibitor AZD8055 (1 μM) or DMSO and increasing doses of 6965. Cells were treated for 72 hr and then collected, stained with PE-AnnexinV, and quantified by FACS analysis. Red numbers indicate the percentage of AnnexinV-positive cells, representing cells actively undergoing apoptosis.

(B) A549 cells were treated with DMSO, 1-μM INK128, 500-nM rapamycin, or 1-μM AZD8055 in the presence or absence of 10-μM 6965 or 10-μM CQ. Cells were treated for 48 hr and then collected, stained with PE-AnnexinV, and quantified by FACS analysis.

(legend continued on next page)

reduce its phosphorylation. Hence, stronger mTOR inhibition, provided by catalytic mTOR inhibitors, is expected to be superior to rapamycin with regards to blocking phosphorylation of ULK1 at the Ser757 mTOR inhibitory site (Kang et al., 2013). Indeed, the extent of apoptosis induced by mTOR inhibitors combined with 6965 thus parallels the ability of these three mTOR drugs to inhibit ULK1 phosphorylation and to induce degradation of the ULK1/Atg13 complex in the presence of 6965. Furthermore, equimolar 6965 was more potent than CQ at inducing apoptosis in combination with all three mTOR drugs (Figures 7B and 7C).

DISCUSSION

Given that the most upstream component of the conserved autophagy cascade encodes the only serine/threonine kinase in the cascade, it has been assumed that ULK1-dependent phosphorylation of other components of the pathway must instruct and provide proper temporal and spatial cues for autophagy initiation. Here, we shed additional light on the complexities involved in the autophagic process by identifying multiple ULK1-dependent phosphorylation sites in Beclin1, Ambra1, Atg101, Syntenin-1, and Vps34. Recent reports that AMPK phosphorylates Beclin1 and Vps34 on distinct sites from these ULK1 sites (Kim et al., 2013) and that the stress-induced MK2/MK3 kinases also target additional sites in Beclin1 (Wei et al., 2015) indicate that much work remains to fully dissect the context-specific, temporal, and spatial differences in the regulation of Vps34/Beclin1 complexes. The induction of ULK1 activity following catalytic mTOR inhibition alone (Figures 4E and S5C) is consistent with amino acid deprivation induction of ULK1 kinase activity, which does not appear to involve AMPK. mTORC1 phosphorylates and inhibits ULK1 via at least one well-established serine site in ULK1, Ser757 (Kang et al., 2013; Kim et al., 2011) and the extent to which different mTOR inhibitors blocked phosphorylation of Ser757 correlated with the ability of 6965 to promote apoptosis. Given that ULK1 is inhibited by mTORC1, further delineation of ULK1 substrate phosphorylation sites may yield valuable biomarkers for mTOR inhibitors, as the attendant increase in ULK1-dependent substrate phosphorylation would be predicted to reflect the relative intensity and effective duration of mTOR inhibition. This appears to be the case, as revealed by endogenous phospho-Atg13 levels in MEFs following starvation or mTOR inhibitor treatment (Figure S5D).

The fact that ULK1 is the only conserved serine/threonine kinase in the autophagy cascade makes it a very attractive target for therapeutic development. Our finding that ULK1 and its binding partner Atg13 are selectively degraded by combining 6965 with starvation or with mTOR inhibitors but not by any of these treatments alone indicates that specifically the active pool of ULK1 kinase complexes may be sensitive to 6965-induced lysosomal degradation. These results provide additional biomarkers for ULK1 inhibition in vivo, as they suggest that ULK1 or Atg13 will be degraded when effectively inhibited by on-target small molecule inhibitors in those cells that rely on ULK1 for survival. Notably, when comparing three mTOR inhibitors for their ability to synergize with 6965 to induce cell death in A549 cells, the extent of apoptosis was paralleled best by loss of Atg13 protein, which in turn mirrored the level of caspase-cleaved PARP. Given the number of ongoing clinical trials combining CQ and CQ analogs with existing cancer therapies, which include mTOR inhibitors (Rangwala et al., 2014), it also worth noting that equimolar 6965 induced more apoptosis than CQ when combined with mTOR inhibitors (Figures 7B and 7C).

Recently, the crystal structure of ATP-competitive kinase inhibitors bound to ULK1 was reported, marking the first report of the ULK1 atomic structure (Lazarus et al., 2015). However, the small molecule inhibitors developed in this study were non-selective, inhibiting tens of kinases >95%, which made them impossible to utilize for cell culture studies (Lazarus et al., 2015). Our study here on 6965 therefore reports one of the first tool compounds that inhibits ULK1 with exquisite selectivity and is suitable for cell studies for the autophagy field. Future efforts will explore the use of this compound and its derivatives in animal models of cancer and other diseases.

mTOR inhibitors are being widely tested in clinical trials for oncology, and rapamycin analogs are the approved standard of care for advanced renal cell carcinoma and other solid tumors (Benjamin et al., 2011). From a therapeutic perspective, an exciting prediction is that ULK1 inhibition will convert the cytostatic response to mTOR inhibition to a cytotoxic response due to loss of autophagic maintenance of cell survival (Figure 7D). We directly tested this hypothesis and found that it holds true in A549 non-small cell lung cancer cells treated with three different mTOR inhibitors (Figure 7). An important step moving forward will be to delineate those tumors that are most likely to show benefit from ULK1 inhibitors like 6965. In hamartoma syndromes, such as tuberous sclerosis complex and Peutz-Jeghers syndrome, inactivating mutations in the tumor suppressors TSC1, TSC2, PTEN, and LKB1/STK11 result in mTOR hyperactivation, and these mutations are targetable by mTOR inhibitors (Bissler et al., 2008). One would hypothesize that the tumors most sensitive to mTOR inhibitors—and hence those perhaps most likely to benefit from dual mTOR/ULK1 inhibition—will be those tumors bearing mutations in genes encoding components of the core mTOR signaling machinery itself (Grabiner et al., 2014). Another possibility is that combining a ULK1 inhibitor such as 6965 with mTOR inhibitors may allow for lower dosing schedules of catalytic mTOR inhibitors. ULK1 inhibition therefore represents an exciting new modality to avoid therapeutic resistance in the many patients currently treated with mTOR inhibitors. The additionally identified ULK1-dependent phosphorylation sites, functional assays, and ULK1 inhibitor tool compound identified in this study will help catalyze further exploration of the roles of this highly conserved autophagy kinase in

(C) Western analysis of A549 cells treated as in 7B. Cellular lysates were immunoblotted with the indicated antibodies.

(D) Model: mTOR inhibitors trigger autophagy by preventing mTOR-dependent inhibitory phosphorylation events on autophagy regulators, including the serine/threonine kinase ULK1. Thus, mTOR inhibition triggers autophagy, which promotes cell survival. Co-administration of an mTOR inhibitor with a ULK1 catalytic inhibitor results in a loss of autophagy induction and prevents the cell survival effect resulting from mTOR inhibition, converting a cytostatic response into a cytotoxic response.

cell biology and in therapeutic possibilities for a wide variety of diseases.

EXPERIMENTAL PROCEDURES

Antibodies and Reagents

Cell Signaling Technology antibodies used were Atg13 (#6940), Beclin1 (#3495), PARP (#9542), 4E-BP1 (#9452), phospho-ULK1 S757 (#6888), ULK1 (#8054), p70 S6K (#9202), phospho-S6 S235/236 (#4858), Myc tag (#2278), LC3B (#3868), Vps34 (#4263), phospho-AMPK T172 (#2535), phospho-ACC S79 (#3661), phospho-Paxillin Y118 (#2541), cleaved caspase 3 (#9664), cleaved caspase 7 (#8438), Src (#2109), IRAK1 (#4504), and PathScan Multiplex Western Cocktail I (#5301). Phospho-Vps34 Ser249 antibody was developed in collaboration with Gary Kasof at Cell Signaling Technology. Sigma antibodies used were ULK1 (A7481), β-actin (A5541), and Flag tag polyclonal (F7425). Gabarap antibody was from Abgent (PM037). Phospho-FAK Y397 was from Abcam (ab4803). FAK was from Epitomics (2146-1). p62 SQSTM1 antibody was from Progen (03-GPP62-C). Phospho-Beclin1 S15 was from Abbiotec (254515). Phospho-Atg13 S318 (human S355) was from Rockland (600-401-C49S). EBSS (14155-063) and glucose-free media (11966-025) were from GIBCO/Life Technologies. Chloroquine (C6628) and bafilomycin A1 (B1793) were from Sigma. MG132 (474790) was from EMD Millipore. AZD-8055 (A-1008) and INK-128 (A-1023) were from Active Biochem. AnnexinV-PE Apoptosis Detection Kit was from BD Biosciences. Phos-tag AAL-107 was from NARD (#304-93521). Ad5-CMV-Cre was purchased from the University of Iowa viral vector core.

SUPPLEMENTAL INFORMATION

Supplemental Information includes Supplemental Experimental Procedures and seven figures and can be found with this article online at http://dx.doi.org/10.1016/j.molcel.2015.05.031.

AUTHOR CONTRIBUTIONS

D.F.E. generated ULK1 for peptide library screening in Figure 1A and performed analysis of all ULK1 substrates and in-depth analysis of Vps34 Ser249 mutant function, comprising all experiments in Figures 2 and 3 except where noted. Experiments in Figures 4, 6, and 7 were performed by D.F.E. and M.G.H.C. D.F.E. performed the in cellulo screen of ULK1 inhibitors that led up to Figure 4C, with compounds synthesized by M.V. and D.R.P., with assistance from D.J.S. and P.T. in the lab of N.D.P.C. H.J.L. in the lab of B.E.T. performed the peptide library screening in Figure 1A, and C.J.M. performed the follow-up peptide analysis in Figure 1C. J.M.A. performed all mass spectrometry analysis contained in Figure 2. H.Z. performed experiments for Figure 5E. J.R. and C.C.Y. performed the RNAi screen of kinases in GFP-LC3 PC3 cells for Figures 5F and 5G. Data in Figure 1 were analyzed by C.J.M., D.F.E., H.J.L., R.J.S., and B.E.T. Data in Figures 2 and 3 were analyzed by D.F.E. and R.J.S. Data in Figures 4 and 5 were analyzed by D.F.E., M.G.H.C., R.J.S., M.V., D.J.S., P.T., and N.D.P.C. Data in Figures 6 and 7 were analyzed by D.F.E., M.G.H.C., and R.J.S. R.J.S. and N.D.P.C. designed the project and guided experiments and analysis of data, with input from all authors. D.F.E., M.G.H.C., and R.J.S. wrote the manuscript with input from B.E.T., D.J.S., P.T., and N.D.P.C.

ACKNOWLEDGMENTS

We thank Dr. Gary Kasof at Cell Signaling Technology for developing the Phospho-VPS34 Ser249 antibody in conjunction with D.F.E. and R.J.S. We thank Drs. Craig Thompson (MSKCC) for the *Ulk1/2* MEFs (Cheong et al., 2011) and Dr. Wei-Xing Zong (SUNY Stony Brook) for the *Vps34*-floxed MEFs (Jaber et al., 2012). We thank Pedro Aza-Blanc in the Functional Genomics core at the Sanford Burnham Medical Research Institute for assistance with the GFP-LC3 quantitation. D.F.E. was supported by the predoctoral T32 CMG training grant to UCSD/Salk. M.G.H.C. was supported by a postdoctoral fellowship from the American Cancer Society (122862-PF-12-258-01-TBG). This work is supported in part by NIH grants R01CA188694 to N.D.P.C., R01GM104047 to B.E.T., and R01CA172229 and Department of Defense (DoD) grant W81XWH-13-1-0043 to R.J.S. Work in the laboratory of R.J.S. was also supported in part through the Howard Hughes Medical Institute, the Salk CCSG P30 CA014195, and the Leona M. and Harry B. Helmsley Charitable Trust grant #2012-PG-MED002.

Received: March 30, 2015
Revised: May 17, 2015
Accepted: May 22, 2015
Published: June 25, 2015

REFERENCES

Benjamin, D., Colombi, M., Moroni, C., and Hall, M.N. (2011). Rapamycin passes the torch: a new generation of mTOR inhibitors. Nat. Rev. Drug Discov. *10*, 868–880.

Bissler, J.J., McCormack, F.X., Young, L.R., Elwing, J.M., Chuck, G., Leonard, J.M., Schmithorst, V.J., Laor, T., Brody, A.S., Bean, J., et al. (2008). Sirolimus for angiomyolipoma in tuberous sclerosis complex or lymphangioleiomyomatosis. N. Engl. J. Med. *358*, 140–151.

Chan, E.Y. (2009). mTORC1 phosphorylates the ULK1-mAtg13-FIP200 autophagy regulatory complex. Sci. Signal. *2*, pe51.

Chan, L.L., Shen, D., Wilkinson, A.R., Patton, W., Lai, N., Chan, E., Kuksin, D., Lin, B., and Qiu, J. (2012). A novel image-based cytometry method for autophagy detection in living cells. Autophagy *8*, 1371–1382.

Cheong, H., Lindsten, T., Wu, J., Lu, C., and Thompson, C.B. (2011). Ammonia-induced autophagy is independent of ULK1/ULK2 kinases. Proc. Natl. Acad. Sci. USA *108*, 11121–11126.

Chresta, C.M., Davies, B.R., Hickson, I., Harding, T., Cosulich, S., Critchlow, S.E., Vincent, J.P., Ellston, R., Jones, D., Sini, P., et al. (2010). AZD8055 is a potent, selective, and orally bioavailable ATP-competitive mammalian target of rapamycin kinase inhibitor with in vitro and in vivo antitumor activity. Cancer Res. *70*, 288–298.

Degtyarev, M., De Maziere, A., Orr, C., Lin, J., Lee, B.B., Tien, J.Y., Prior, W.W., van Dijk, S., Wu, H., Gray, D.C., et al. (2008). Akt inhibition promotes autophagy and sensitizes PTEN-null tumors to lysosomotropic agents. J. Cell. Biol. *183*, 101–116.

Egan, D., Kim, J., Shaw, R.J., and Guan, K.L. (2011a). The autophagy initiating kinase ULK1 is regulated via opposing phosphorylation by AMPK and mTOR. Autophagy *7*, 643–644.

Egan, D.F., Shackelford, D.B., Mihaylova, M.M., Gelino, S., Kohnz, R.A., Mair, W., Vasquez, D.S., Joshi, A., Gwinn, D.M., Taylor, R., et al. (2011b). Phosphorylation of ULK1 (hATG1) by AMP-activated protein kinase connects energy sensing to mitophagy. Science *331*, 456–461.

Fabian, M.A., Biggs, W.H., 3rd, Treiber, D.K., Atteridge, C.E., Azimioara, M.D., Benedetti, M.G., Carter, T.A., Ciceri, P., Edeen, P.T., Floyd, M., et al. (2005). A small molecule-kinase interaction map for clinical kinase inhibitors. Nat. Biotechnol. *23*, 329–336.

Goodwin, J.M., Svensson, R.U., Lou, H.J., Winslow, M.M., Turk, B.E., and Shaw, R.J. (2014). An AMPK-independent signaling pathway downstream of the LKB1 tumor suppressor controls Snail1 and metastatic potential. Mol. Cell. *55*, 436–450.

Grabiner, B.C., Nardi, V., Birsoy, K., Possemato, R., Shen, K., Sinha, S., Jordan, A., Beck, A.H., and Sabatini, D.M. (2014). A diverse array of cancer-associated MTOR mutations are hyperactivating and can predict rapamycin sensitivity. Cancer Discov *4*, 554–563.

Green, D.R., and Levine, B. (2014). To be or not to be? How selective autophagy and cell death govern cell fate. Cell *157*, 65–75.

Guo, J.Y., Chen, H.Y., Mathew, R., Fan, J., Strohecker, A.M., Karsli-Uzunbas, G., Kamphorst, J.J., Chen, G., Lemons, J.M., Karantza, V., et al. (2011). Activated Ras requires autophagy to maintain oxidative metabolism and tumorigenesis. Genes Dev. *25*, 460–470.

Guo, J.Y., Xia, B., and White, E. (2013). Autophagy-mediated tumor promotion. Cell *155*, 1216–1219.

Gwinn, D.M., Shackelford, D.B., Egan, D.F., Mihaylova, M.M., Mery, A., Vasquez, D.S., Turk, B.E., and Shaw, R.J. (2008). AMPK phosphorylation of raptor mediates a metabolic checkpoint. Mol. Cell *30*, 214–226.

Hosokawa, N., Sasaki, T., Iemura, S., Natsume, T., Hara, T., and Mizushima, N. (2009). Atg101, a novel mammalian autophagy protein interacting with Atg13. Autophagy *5*, 973–979.

Hsieh, A.C., Liu, Y., Edlind, M.P., Ingolia, N.T., Janes, M.R., Sher, A., Shi, E.Y., Stumpf, C.R., Christensen, C., Bonham, M.J., et al. (2012). The translational landscape of mTOR signalling steers cancer initiation and metastasis. Nature *485*, 55–61.

Jaber, N., Dou, Z., Chen, J.S., Catanzaro, J., Jiang, Y.P., Ballou, L.M., Selinger, E., Ouyang, X., Lin, R.Z., Zhang, J., and Zong, W.X. (2012). Class III PI3K Vps34 plays an essential role in autophagy and in heart and liver function. Proc. Natl. Acad. Sci. USA *109*, 2003–2008.

Jiang, X., Overholtzer, M., and Thompson, C.B. (2015). Autophagy in cellular metabolism and cancer. J. Clin. Invest. *125*, 47–54.

Kang, S.A., Pacold, M.E., Cervantes, C.L., Lim, D., Lou, H.J., Ottina, K., Gray, N.S., Turk, B.E., Yaffe, M.B., and Sabatini, D.M. (2013). mTORC1 phosphorylation sites encode their sensitivity to starvation and rapamycin. Science *341*, 1236566.

Karaman, M.W., Herrgard, S., Treiber, D.K., Gallant, P., Atteridge, C.E., Campbell, B.T., Chan, K.W., Ciceri, P., Davis, M.I., Edeen, P.T., et al. (2008). A quantitative analysis of kinase inhibitor selectivity. Nat. Biotechnol. *26*, 127–132.

Karsli-Uzunbas, G., Guo, J.Y., Price, S., Teng, X., Laddha, S.V., Khor, S., Kalaany, N.Y., Jacks, T., Chan, C.S., Rabinowitz, J.D., et al. (2014). Autophagy is required for glucose homeostasis and lung tumor maintenance. Cancer Discov *4*, 914–927.

Kim, Y.C., and Guan, K.L. (2015). mTOR: a pharmacologic target for autophagy regulation. J. Clin. Invest. *125*, 25–32.

Kim, J., Kundu, M., Viollet, B., and Guan, K.L. (2011). AMPK and mTOR regulate autophagy through direct phosphorylation of Ulk1. Nat. Cell Biol. *13*, 132–141.

Kim, J., Kim, Y.C., Fang, C., Russell, R.C., Kim, J.H., Fan, W., Liu, R., Zhong, Q., and Guan, K.L. (2013). Differential regulation of distinct Vps34 complexes by AMPK in nutrient stress and autophagy. Cell *152*, 290–303.

Kinoshita, E., Kinoshita-Kikuta, E., Takiyama, K., and Koike, T. (2006). Phosphate-binding tag, a new tool to visualize phosphorylated proteins. Mol. Cell. Proteomics *5*, 749–757.

Konno, H., Konno, K., and Barber, G.N. (2013). Cyclic dinucleotides trigger ULK1 (ATG1) phosphorylation of STING to prevent sustained innate immune signaling. Cell *155*, 688–698.

Kroemer, G. (2015). Autophagy: a druggable process that is deregulated in aging and human disease. J. Clin. Invest. *125*, 1–4.

Lazarus, M.B., Novotny, C.J., and Shokat, K.M. (2015). Structure of the human autophagy initiating kinase ULK1 in complex with potent inhibitors. ACS Chem. Biol. *10*, 257–261.

Li, J., Kim, S.G., and Blenis, J. (2014). Rapamycin: one drug, many effects. Cell Metab. *19*, 373–379.

Mercer, C.A., Kaliappan, A., and Dennis, P.B. (2009). A novel, human Atg13 binding protein, Atg101, interacts with ULK1 and is essential for macroautophagy. Autophagy *5*, 649–662.

Miller, M.L., Jensen, L.J., Diella, F., Jørgensen, C., Tinti, M., Li, L., Hsiung, M., Parker, S.A., Bordeaux, J., Sicheritz-Ponten, T., et al. (2008). Linear motif atlas for phosphorylation-dependent signaling. Sci. Signal. *1*, ra2.

Obenauer, J.C., Cantley, L.C., and Yaffe, M.B. (2003). Scansite 2.0: Proteome-wide prediction of cell signaling interactions using short sequence motifs. Nucleic Acids Res. *31*, 3635–3641.

Papinski, D., Schuschnig, M., Reiter, W., Wilhelm, L., Barnes, C.A., Maiolica, A., Hansmann, I., Pfaffenwimmer, T., Kijanska, M., Stoffel, I., et al. (2014). Early steps in autophagy depend on direct phosphorylation of Atg9 by the Atg1 kinase. Mol. Cell *53*, 471–483.

Rajesh, S., Bago, R., Odintsova, E., Muratov, G., Baldwin, G., Sridhar, P., Rajesh, S., Overduin, M., and Berditchevski, F. (2011). Binding to syntenin-1 protein defines a new mode of ubiquitin-based interactions regulated by phosphorylation. J. Biol. Chem. *286*, 39606–39614.

Rangwala, R., Chang, Y.C., Hu, J., Algazy, K.M., Evans, T.L., Fecher, L.A., Schuchter, L.M., Torigian, D.A., Panosian, J.T., Troxel, A.B., et al. (2014). Combined MTOR and autophagy inhibition: phase I trial of hydroxychloroquine and temsirolimus in patients with advanced solid tumors and melanoma. Autophagy *10*, 1391–1402.

Russell, R.C., Tian, Y., Yuan, H., Park, H.W., Chang, Y.Y., Kim, J., Kim, H., Neufeld, T.P., Dillin, A., and Guan, K.L. (2013). ULK1 induces autophagy by phosphorylating Beclin-1 and activating VPS34 lipid kinase. Nat. Cell Biol. *15*, 741–750.

Sun, S.Y., Rosenberg, L.M., Wang, X., Zhou, Z., Yue, P., Fu, H., and Khuri, F.R. (2005). Activation of Akt and eIF4E survival pathways by rapamycin-mediated mammalian target of rapamycin inhibition. Cancer Res. *65*, 7052–7058.

Tsukada, M., and Ohsumi, Y. (1993). Isolation and characterization of autophagy-defective mutants of Saccharomyces cerevisiae. FEBS Lett. *333*, 169–174.

Turk, B.E. (2008). Understanding and exploiting substrate recognition by protein kinases. Curr. Opin. Chem. Biol. *12*, 4–10.

Wei, Y., An, Z., Zou, Z., Sumpter, R., Su, M., Zang, X., Sinha, S., Gaestel, M., and Levine, B. (2015). The stress-responsive kinases MAPKAPK2/MAPKAPK3 activate starvation-induced autophagy through Beclin 1 phosphorylation. eLife *4*, e05289.

White, E. (2015). The role for autophagy in cancer. J. Clin. Invest. *125*, 42–46.

Molecular Cell, Volume *59*

Supplemental Information

Small Molecule Inhibition of the Autophagy Kinase ULK1 and Identification of ULK1 Substrates

Daniel F. Egan, Matthew G.H. Chun, Mitchell Vamos, Haixia Zou, Juan Rong, Chad J. Miller, Hua Jane Lou, Dhanya Raveendra-Panickar, Chih-Cheng Yang,Douglas J. Sheffler, Peter Teriete, John M. Asara, Benjamin E. Turk, Nicholas D.P. Cosford, and Reuben J. Shaw

A

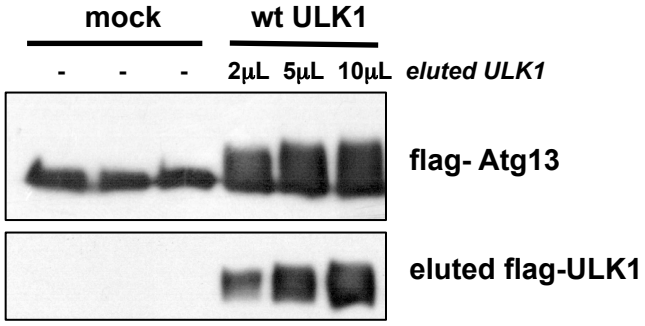

Figure S1. Flag-tagged ULK1 is catalytically active as determined by an in vitro kinase assay using Atg13 as a substrate, related to Figure 1

(A) Wild-type Flag-tagged ULK1 (WT ULK1) was transfected into human embryonic kidney (HEK-293T) cells and immunoprecipitated 24 hours post-transfection with M2 agarose. The immunoprecipitated WT ULK1 was eluted using 3X Flag peptide and subsequently used in an in vitro kinase assay using wild-type Flag-tagged Atg13 (Flag-Atg13) as a substrate. Flag-Atg13 was generated in the same manner from parallel plates of HEK-293T cells. A mobility shift is indicative of phosphorylation.

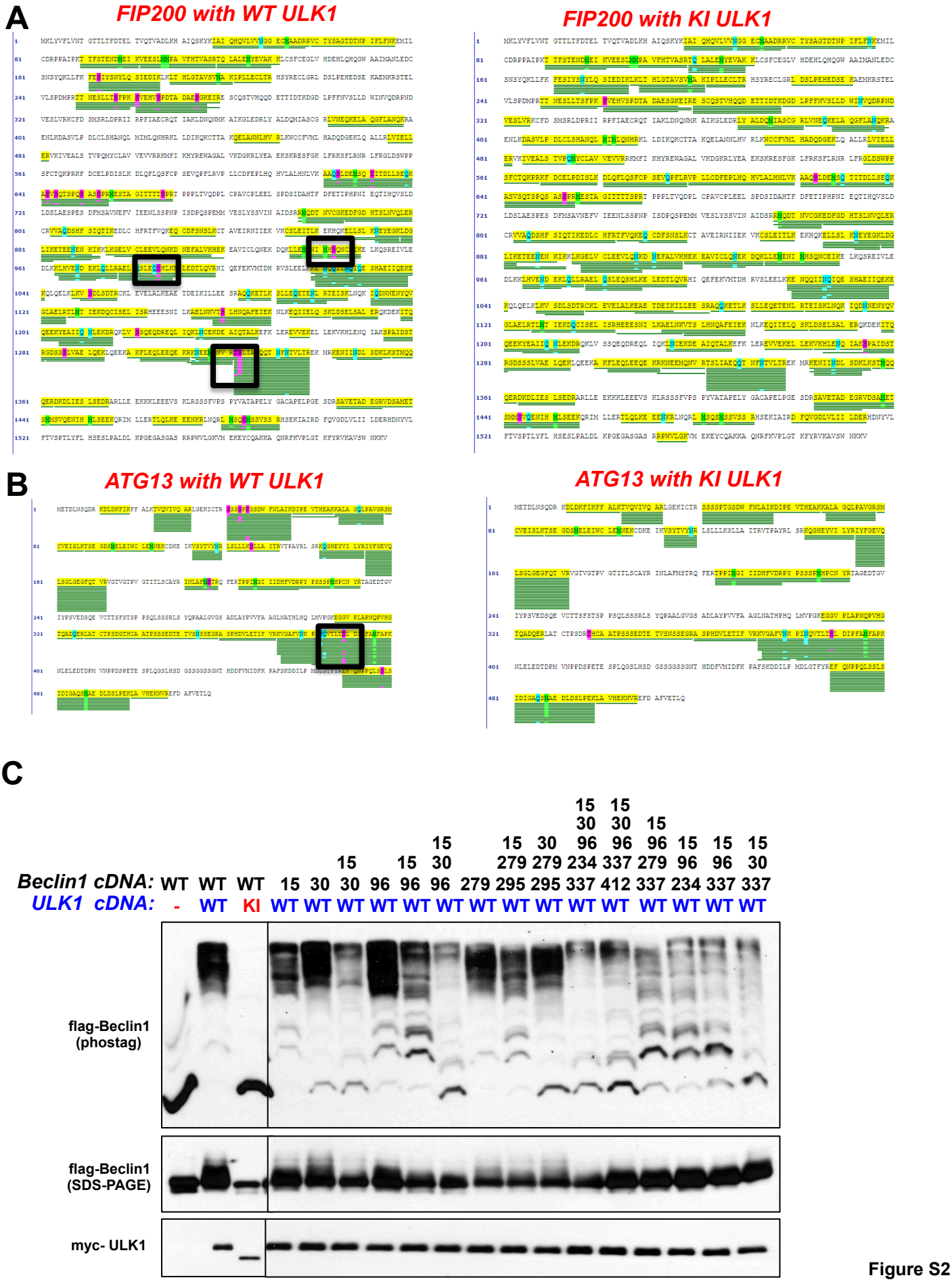
A
FIP200 with WT ULK1
FIP200 with KI ULK1
B
ATG13 with WT ULK1
ATG13 with KI ULK1
C
Beclin1 cDNA: WT WT WT 15 30 30 96 96 96 279 295 295 337 412 337 234 337 337
ULK1 cDNA: - WT KI WT WT WT WT WT WT WT WT WT WT WT WT WT WT WT WT
flag-Beclin1 (phostag)
flag-Beclin1 (SDS-PAGE)
myc- ULK1

Figure S2

Figure S2. Identification of ULK1-dependent in vivo phosphorylation sites in FIP200, Atg13, and Beclin1, related to Figure 2.

(A) Diagram of all LC/MS/MS identified in vivo phosphorylation sites in human FIP200. Myc-tagged wild-type ULK1 (WT ULK1; left) or Myc-tagged kinsase-inactive ULK1 (KI ULK1; right) was transfected into HEK-293T cells along with wild-type Flag-tagged FIP200 (FIP200) and immunoprecipitated with M2 agarose. The immunoprecipitate was run out on an SDS-PAGE gel, stained with coomassie, and the band corresponding to FIP200 was cut out, isolated, and subjected to tryptic digest and LC/MS/MS analysis. The phosphorylated sites that conform to the optimal ULK1 phosphorylation motif that were identified by this analysis are boxed. Green bars indicate peptide coverage, and purple highlights indicate phosphorylation events.

(B) Diagram of all LC/MS/MS identified in vivo phosphorylation sites in human Atg13
Same as S2A except using wild-type Flag-tagged Atg13 (Atg13) as a substrate.

(C) ULK1-dependent bandshifts in Beclin 1. WT ULK1 or KI ULK1 was transfected into HEK-293T cells along with wild-type Flag-tagged Beclin 1 or Flag-tagged Beclin 1 serine-to-alanine point-mutants. The specific mutants used in this analysis are indicated by the position(s) of the substituted amino acid (top). Cellular lysates were isolated 24 hours post-transfection, run on an SDS-PAGE gel containing the Phos-Tag reagent (middle) or a standard SDS-PAGE gel lacking the Phos-Tag reagent (bottom), and transferred to PVDF membranes, which were subsequently probed with the indicated antibodies.

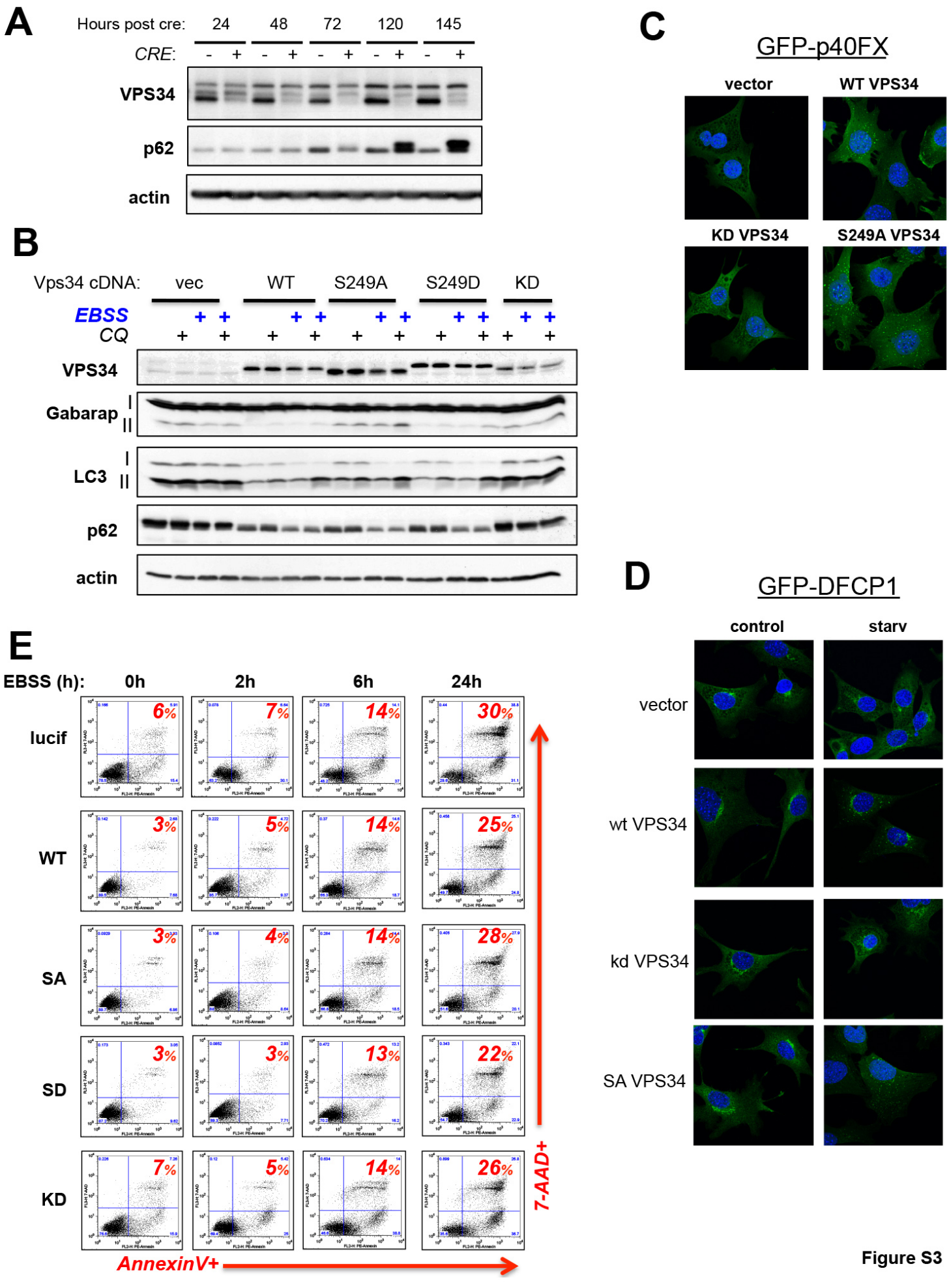
A
Hours post cre: 24 48 72 120 145
CRE: - + - + - + - + - +
VPS34
p62
actin
B
Vps34 cDNA: vec WT S249A S249D KD
EBSS + + + + + + + + + +
CQ + + + + + + + + + +
VPS34
Gabarap I II
LC3 I II
p62
actin
C
GFP-p40FX
vector
WT VPS34
KD VPS34
S249A VPS34
D
GFP-DFCP1
control
starv
vector
wt VPS34
kd VPS34
SA VPS34
E
EBSS (h): 0h 2h 6h 24h
lucif 6% 7% 14% 30%
WT 3% 5% 14% 25%
SA 3% 4% 14% 28%
SD 3% 3% 13% 22%
KD 7% 5% 14% 26%
7-AAD+
AnnexinV+

Figure S3

Figure S3. Vps34 Ser249 does not appear critical in Vps34 functional assays, related to Figure 3.
(A) Conditional deletion of Vps34 in MEFs results in reduced autophagic flux. Mouse embryonic fibroblasts (MEFs) derived from $Vps34^{flox/flox}$ mice were treated with adenovirus encoding Cre recombinase (Ad-Cre; MOI of 100) for the indicated times to delete the endogenous VSP34 gene. Cellular lysates were immunoblotted with the indicated antibodies.
(B) Vps34 Ser249 is not required for LC3 lipidation or p62 degradation during starvation conditions. $Vps34^{flox/flox}$ MEFs were stably reconstituted with wild-type Flag-tagged Vps34 (WT) or Flag-tagged Vps34 mutants using retrovirus (vec: empty vector; serine-to-alanine: S249A; serine-to-aspartate: S249D; kinase inactive: KD). Stably reconstituted cells were treated with Ad-Cre (as in S3A). 48 hours post-adenovirus treatment, cells were treated with fresh media (Dulbecco's modified Eagle medium [DMEM] containing 10% fetal bovine serum [FBS]) or starvation media (Earle's balanced salt solution [EBSS]) in the presence or absence of 20 μM chloroquine (CQ) for two hours. Cellular lysates were immunoblotted with the indicated antibodies.
(C) Vps34 Ser249 is not required for p40FX puncta. $Vps34^{flox/flox}$ MEFs stably reconstituted with WT Vps34 or Vps34 mutants (from S3B) were stably transduced with GFP-p40FX using lentivirus. Cells were treated with Ad-Cre (as in S3A). 48 hours post-adenovirus treatment, cells were fixed and analyzed by confocal microscopy for the presence of GFP-p40FX puncta.
(D) Vps34 Ser249 is not required for DFCP1 puncta. $Vps34^{flox/flox}$ MEFs stably reconstituted with WT Vps34 or Vps34 mutants (from S3B) were stably transduced with GFP-DFCP1 using lentivirus. Cells were treated with Ad-Cre (as in S3A). 48 hours post-adenovirus treatment, cells were treated with fresh media or starvation media (as in S3B) for two hours and then fixed and analyzed by confocal microscopy for the presence of GFP-DFCP1 puncta.
(E) Vps34 Ser249 is not required for MEFs to survive periods of starvation. $Vps34^{flox/flox}$ MEFs stably reconstituted with WT Vps34 or Vps34 mutants (from S3B) were treated with Ad-Cre (as in S3A). 48 hours post-adenovirus treatment, cells were treated with fresh media or starvation media (as in S3B) for 2, 6, or 24 hours. Cells were collected, stained with 7-AAD and PE-AnnexinV, and quantified for apoptosis by fluorescence-activated cell sorting (FACS) analysis. Red numbers indicate the percentage of 7-AAD/PE-AnnexinV double-positive cells, representative of end-stage apoptosis and death.

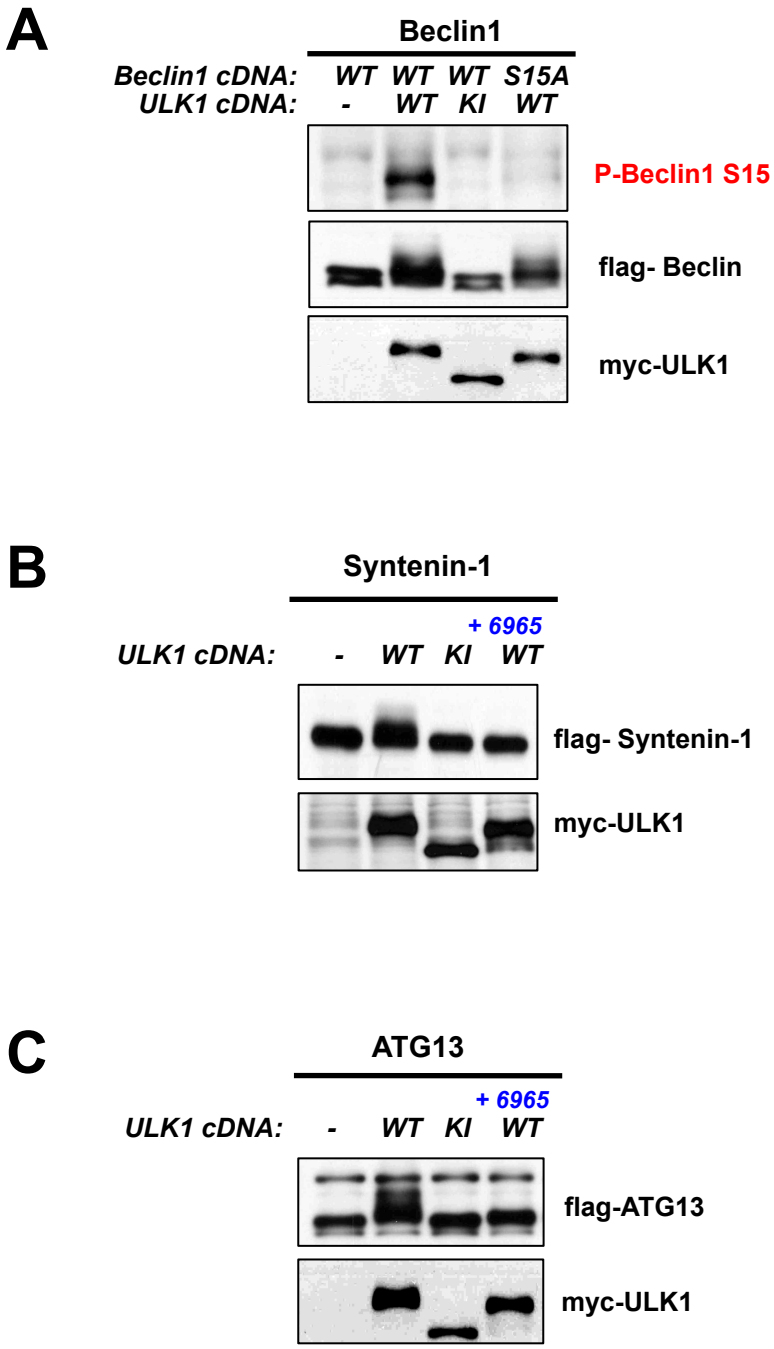

Figure S4. Phosphorylation of multiple substrates of ULK1 are inhibited in cells by treatment with SBI-0206965, related to Figure 4.

(A) HEK-293T cells were transfected with a wild-type Flag-tagged Beclin1 (Beclin1 WT) or a Flag-tagged serine-to-alanine mutant Beclin1 (Beclin1 S15A) and WT ULK1 or KI ULK1. Cellular lysates were isolated 24 hours post-transfection and immunoblotted with the indicated antibodies.

(B) HEK-293T cells were transfected with wild-type Flag-tagged Syntenin-1 and wild-type (WT) or kinase-inactive (KI) Myc-tagged ULK1. 24 hours post-transfection, cells were treated with or without SBI-0206965 (10 μM) for 1 hour. Cell lysates were probed with the indicated antibodies. A mobility shift is indicative of phosphorylation in Flag-Syntenin-1.

(C) Same as S4B except using wild-type Flag-tagged Atg13. Mobility shift is indicative of phosphorylation in Flag-Atg13.

A

Compound Name	Selectivity Score Type	Number of Hits	Number of Non-Mutant Kinases	Screening Concentration (nM)	Selectivity Score
SBI-0206965.0003	S(35)	49	397	1000	0.123
SBI-0206965.0003	S(10)	19	397	1000	0.048
SBI-0206965.0003	S(1)	4	397	1000	0.010

B

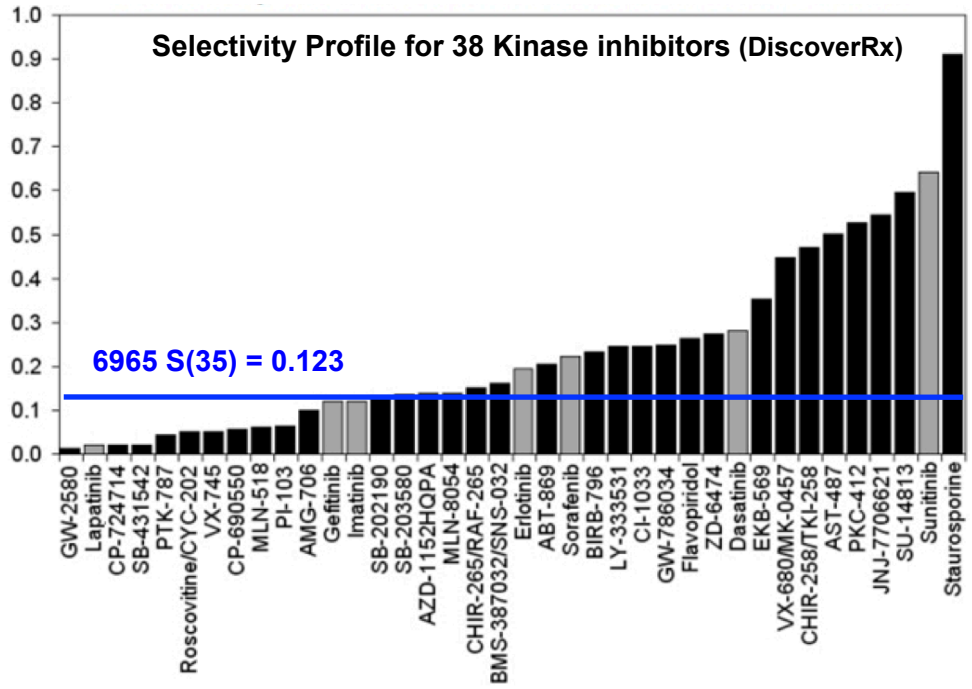

C

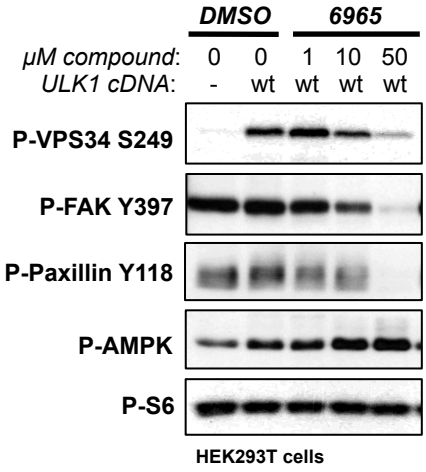

D

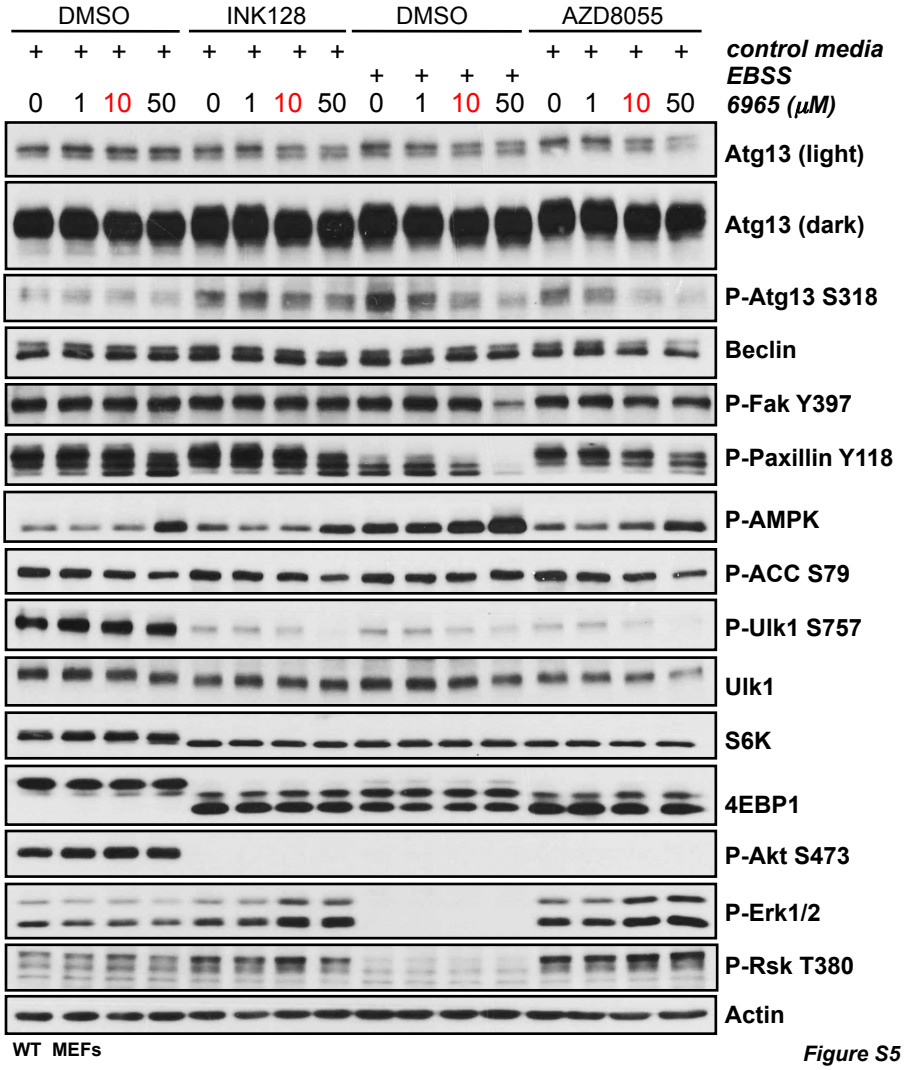

E

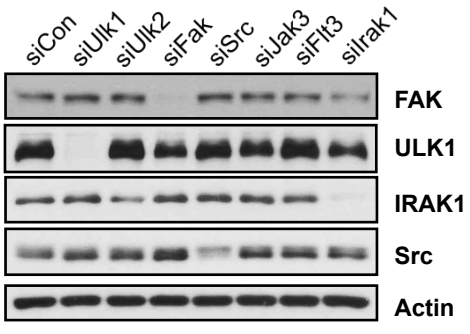

Figure S5

Figure S5. SBI-0206965 is a highly selective kinase inhibitor, related to Figure 5.
(A) Kinase activity was measured against a diverse panel of kinases as seen in Figure 5A and 5B. Selectivity Scores (S-score) were determined for SBI-0206965. Compound selectivity is calculated by dividing the number of kinases whose binding is inhibited below a certain threshold relative to the negative DMSO control by the total number of distinct kinases tested. For example, S(35) represents the fraction of tested kinases whose binding was inhibited to less than 35% of the DMSO negative control.
(B) Comparison of Selectivity Scores for SBI-0206965 versus a panel of clinically relevant kinase inhibitors. S(35) Selectivity Score for SBI-0206965 relative to the S(35) Selectivity Scores for a panel of 38 clinically relevant kinase inhibitors (adapted from DiscoverRx data).
(C) HEK-293T cells were transfected with wild-type ULK1 (wt). 24 hours later, cells were treated with indicated doses of SBI-0206965 for 1 hour. Cell lysates were immunoblotted with the indicated antibodies.
(D) Wild-type mouse embryonic fibroblasts (MEFs) were treated with fresh media (Dulbecco's modified Eagle medium [DMEM] containing 10% fetal bovine serum [FBS]) containing 1 μM INK128, 1 μM AZD8055, or DMSO or with starvation media (Earle's balanced salt solution [EBSS] in the presence of 6965 in a dose response manner (0, 1, 10, and 50 μM). Cellular lysates were isolated after 1 hour of treatment and immunoblotted with the indicated antibodies.
(E) PC3 human prostate cells that stably express a construct encoding LC3 fused to green fluorescent protein (GFP-LC3) were transfected with siRNAs against indicated kinases. Cellular lysates were isolated 48 hours after RNAi transfection and immunoblotted with the indicated antibodies.

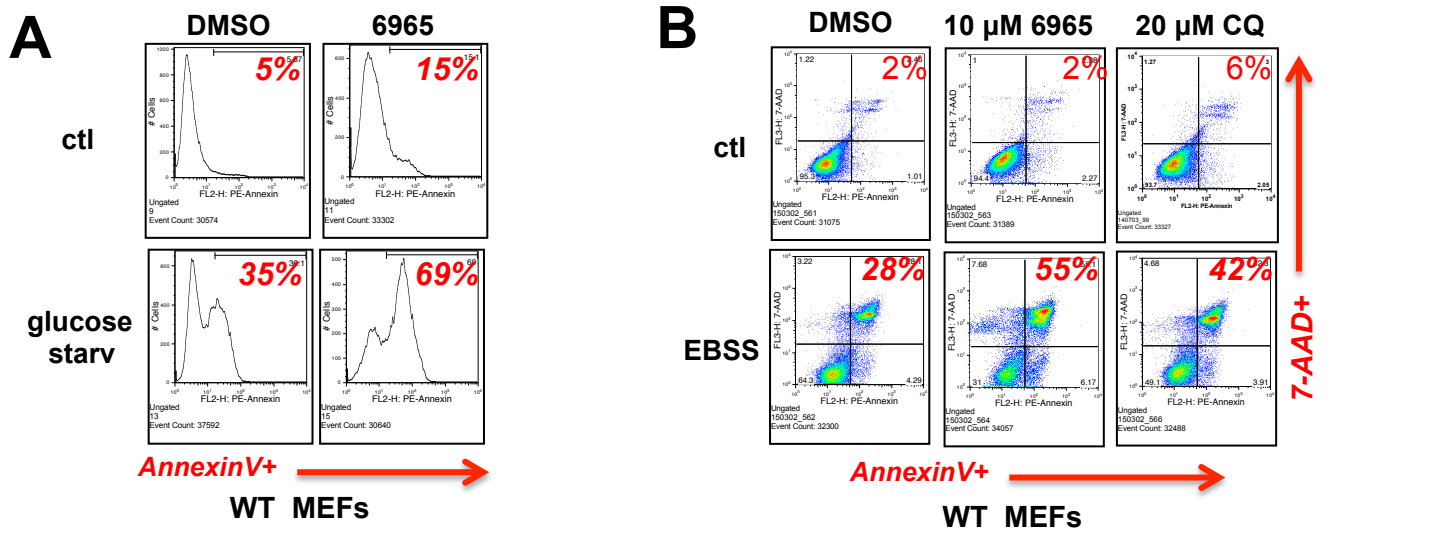
A
DMSO
6965
ctl
glucose starv
5%
15%
35%
69%
AnnexinV+
WT MEFs
B
DMSO
10 μM 6965
20 μM CQ
ctl
EBSS
2%
2%
6%
28%
55%
42%
7-AAD+
AnnexinV+
WT MEFs

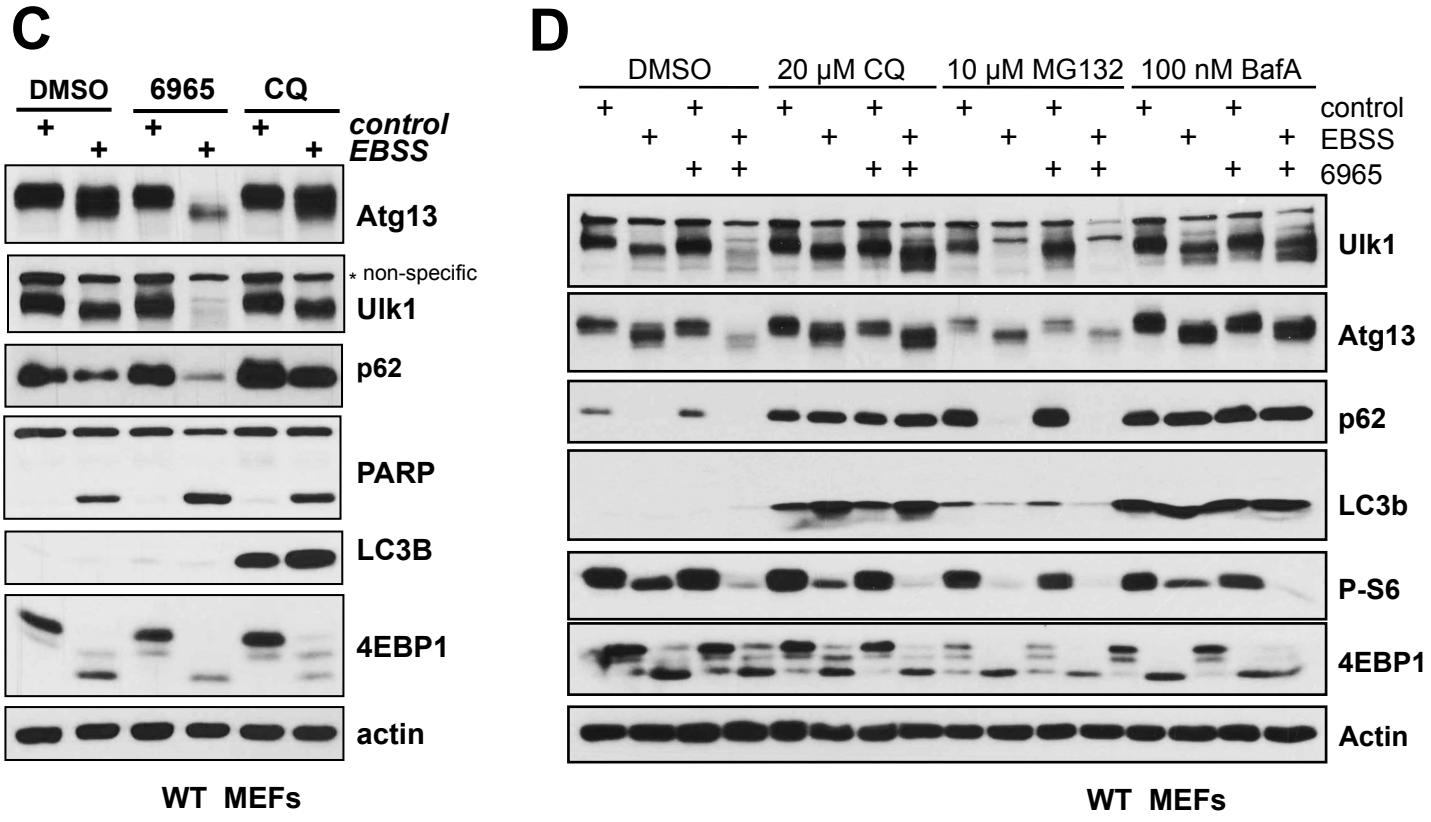
C
DMSO
6965
CQ
control
EBSS
Atg13
* non-specific
Ulk1
p62
PARP
LC3B
4EBP1
actin
WT MEFs
D
DMSO
20 μM CQ
10 μM MG132
100 nM BafA
control
EBSS
6965
Ulk1
Atg13
p62
LC3b
P-S6
4EBP1
Actin
WT MEFs

Figure S6

Figure S6. Starvation synergizes with SBI-0206965 to enhance apoptosis in different cell types, related to Figure 6.

(A) Glucose starvation synergizes with SBI-0206965 to induce an enhanced apoptotic response in MEFs. Wild-type mouse embryonic fibroblasts (MEFs) were treated with fresh media (Dulbecco's modified Eagle medium [DMEM] containing 10% dialyzed fetal bovine serum [FBS]) or the same media lacking glucose and 10 μM SBI-0206965 or DMSO for 18 hours. Cells were collected, stained with 7-AAD and PE-AnnexinV, and quantified for apoptosis by fluorescence-activated cell sorting (FACS) analysis. Red numbers indicate the percentage of 7-AAD/PE-AnnexinV double-positive cells, representative of end-stage apoptosis and death.

(B) Starvation synergizes with SBI-0206965 to induce an enhanced apoptotic response in MEFs as compared to the autophagy inhibitor chloroquine. Wild-type MEFs were treated with fresh media or starvation media (Earle's balanced salt solution [EBSS]) and 10 μM SBI-0206965, 20 μM chloroquine (CQ), or DMSO for 14 hours. Cells were collected, stained with 7-AAD and PE-AnnexinV, and quantified for apoptosis by fluorescence-activated cell sorting (FACS) analysis. Red numbers indicate the percentage of 7-AAD/PE-AnnexinV double-positive cells, representative of end-stage apoptosis and death.

(C) Western analysis of wild-type MEFs treated as in S6B. Cellular lysates were immunoblotted with the indicated antibodies.

(D) Wild-type MEFs were treated with fresh media (Dulbecco's modified Eagle medium [DMEM] containing 10% fetal bovine serum [FBS]) or with starvation media (Earle's balanced salt solution [EBSS]) containing 20 μM chloroquine (CQ), 10 μM MG132, 100 nM bafilomycin A (BafA), or DMSO in the presence or absence of 10 μM 6965. Cellular lysates were isolated after 14 hours of treatment and immunoblotted with the indicated antibodies.

A

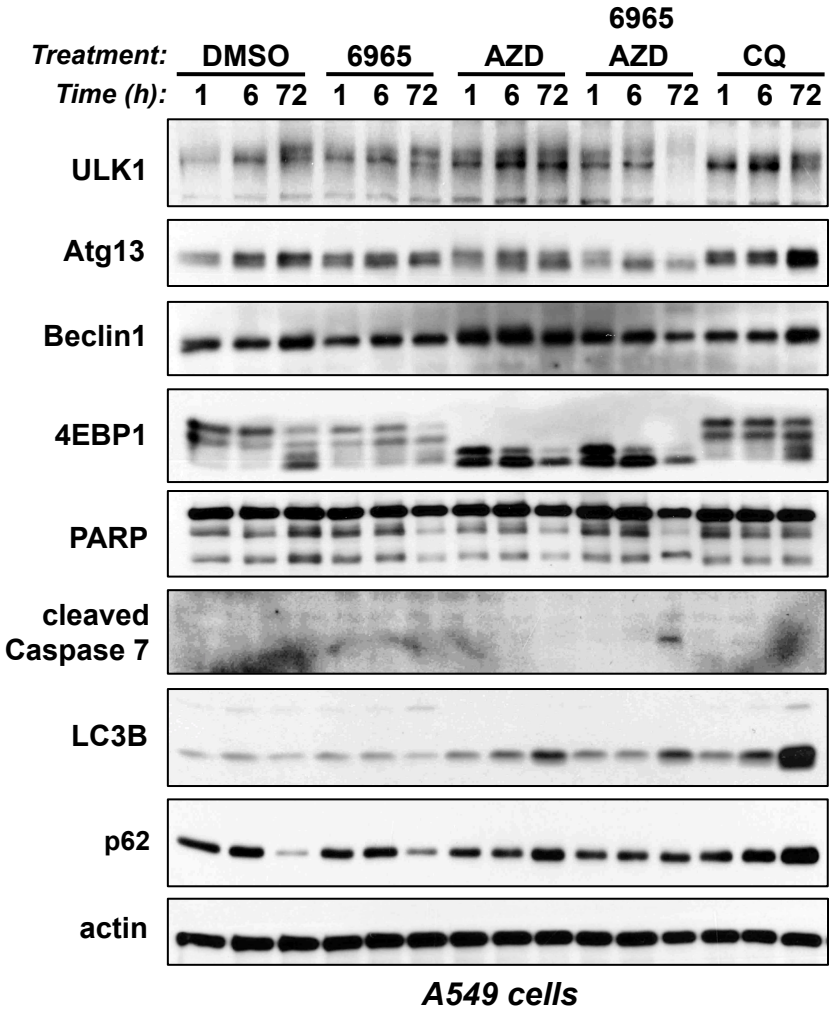

Figure S7. SBI-0206965 synergizes with the mTOR catalytic inhibitor AZD8055 to induce an enhanced apoptotic response in A549 non-small cell lung cancer cells, related to Figure 7.
(A) A549 cells were treated with DMSO, 10 μM SBI-0206965, 1 μM AZD8055, 10 μM SBI-0206965 and 1 μM AZD8055, or 20 μM chloroquine (CQ) for 1, 6, or 72 hours. Cellular lysates were immunoblotted with the indicated antibodies.

SUPPLEMENTAL MATERIALS

SUPPLEMENTAL EXPERIMENTAL PROCEDURES

Plasmids

The cDNA encoding human Atg13 (KIAA0652/AB014552) was obtained from Kazusa DNA Research Institute in Japan. The cDNAs encoding human FIP200, mouse ULK1, and mouse ULK2 were obtained from Open Biosystems (clones 3908134, 6834534, and 5709559 respectively). The cDNAs encoding human Atg101, human Vps34, human Ambra1, and human Beclin1 were obtained from Invitrogen. The cDNA for mouse Syntenin-1 was cloned from a cDNA library prepared from mouse embryonic fibroblasts (MEFs) and sequence verified to match the sequence of the transcript variant 1 of mouse Syntenin-1 (NM_001098227.1).

The Flag tag and attL1 sites (for BP reaction) were cloned by PCR using standard methods. cDNAs were subcloned into pDONR221 with BP clonase (Invitrogen), and site-directed mutagenesis was performed using QuikChange II XL (Stratagene). Kinase dead ULK1 was achieved by introduction of a K46I mutation. Kinase dead Vps34 was achieved by introduction of a D747N/N748K double mutation. Wild-type and mutant alleles in pDONR221 were sequenced in their entirety to verify no additional mutations were introduced during PCR or mutagenesis steps and then put into either pcDNA3 Myc or pcDNA3 Flag mammalian expression vectors, or pcDNA6.2 V5 destination vector (Invitrogen), or pQCXIN retroviral destination vector (Addgene 17399) by LR reaction (Invitrogen). pMXs-puro-GFP-DFCP1 was a kind gift from Noboru Mizushima (University of Tokyo) and pEGFP-p40PX was a kind gift from Seth Field (UCSD).

Cell culture, transient transfections, cell lysis and Phos-tag™ mobility shift analysis

HEK-293T, U87MG, PC3, A549, and SV40 immortalized wild-type mouse embryonic fibroblast (MEF) cells were cultured in DMEM (Mediatech) containing 10% fetal bovine serum (Hyclone, Thermo Scientific) and penicillin/streptomycin at 37°C in 10% CO_2. *Ulk*1/2 DKO MEFs and controls were a kind gift from Craig Thompson (MSKCC). Vps34$^{flox/flox}$ MEFs from Wei-Xing Zong (SUNYSB). For transient expression in HEK-293T cells, cells were transfected with 2 μg each DNA plasmid per 6 cm dish using Lipofectamine 2000 (Invitrogen) following the manufacturer's protocol. Cells were harvested 24 hours after transfection and cell lysates were prepared and immunoblotted as previously described (Egan et al., 2011). Phos-tag™ gels were prepared according to the manufacturers instructions. Briefly, Phos-tag™ AAL-107 was added to the SDS-PAGE acryamide mixture at a final concentration of 50 μM along with $MnCl_2$ at a final concentration of 100 μM. Prior to transfer, the gel

was soaked in transfer buffer containing 1 mM EDTA for 30 minutes with gentle agitation to eliminate the manganese ions from the gel. The gel was subsequently transfered to PVDF membranes and probed with indicated antibodies according to the manufacturers instructions.

***Establishment and study of autophagy induction in PC3 cells stably expressing GFP-LC3*.**

PC3 cells were propagated and maintained at 37°C in a humidified 5% CO_2/95% air atmosphere incubator in RPMI 1640 medium (Cellgro) supplemented with 2 mM glutamine, 10% fetal bovine serum (FBS; Sigma), 100 IU/ml penicillin, and 100 µg/ml streptomycin. Transfection was carried out using lipofectamine 2000 (Life Technologies). Briefly, PC3 cells were cultured overnight and then transfected with pBABE-GFP-LC3-puro and lipofectamine 2000 mix in Opti-MEM I reduced serum medium (Life Technologies) at a 1:1 (µg:µl) ratio. The next day, cells were seeded in a 6-well plate at varying cell densities and selected with 1 µg/ml puromycin in 10% FBS/RPMI. Puromycin-resistant cell clones were maintained in 10% FBS/RPMI containing 1 µg/ml puromycin. Under normal culture conditions, GFP-LC3 showed diffuse cytoplasmic distribution in PC3 cells. PC3 cell clone 2 was selected for further experiments and named PC3-GFP-LC3.

High-content imaging analysis and siRNA genetic screening in PC3-GFP-LC3 cells*.*

PC3-GFP-LC3 cells were dispensed at a cell density of 2000 cells and 20,000 cells per well in black/clear 384-well plates (Greiner # 781091) or 96-well plates (Greiner # 655946) respectively and were treated with siRNAs or compounds as described. The cells were subsequently fixed with 4% paraformaldehyde and counter-stained with 0.1 µg/ml DAPI (Thermo Scientific) to reveal nuclei. The cells were imaged with an Opera high-content screening system (PerkinElmer) using a 40X objective to visualize GFP-LC3 proteins and the nuclei. 8 and 16 images were obtained from different fields in each well for 384-well plates and 96-well plates, respectively. The images were analyzed with the Acapella high-content imaging and analysis software for valid cell numbers per field, average autophagosomal spot intensity per cell, average number of autophagosomal spots per cell, and autophagosomal spot area per cell. PC3-GFP-LC3 cells treated with DMSO or autophagy inducers (AZD8055 and INK128) served as negative and positive imaging controls respectively. siRNA pools for target genes were selected from the genome-wide ON-TARGET-Plus Human siRNA library (Dharmacon/Thermo Scientific) and tested in duplicates. 1 µl of 0.5 µM siRNA pools, 0.1 µl RNAiMAX reagent, and 8.9 µl Opti-MEM (Life Technologies) were spotted into the black/clear 384-well plates. 40 µl of PC3-GFP-LC3 cells were dispensed into the pre-spotted 384-well plates at a cell density of 2000 cells per well and reverse-transfected with 10 nM siRNA pools containing four individual 2.5 nM siRNAs for a target gene. 48 hours after transfection, cells were treated with DMSO control, 1 µM

AZD 8055, or 1 μM INK128 as indicated for 4 hours. The cells were then fixed, counter-stained with DAPI, and analyzed by high-content imaging. The siRNAs pools containing 48 non-targeting siRNAs (Dharmacon) were used as a negative control. Killer siRNA (EIF4A3 siRNA, Ambion) served as a transfection efficiency control. Hits were defined based upon the criteria of ≥50% inhibition of the number of autophagosomal spots per cell induced by both AZD8055 and INK128 in duplicates.

Peptide kinase assays

For peptide library screening, ULK1/FIP200/Atg13 complexes were used to phosphorylate peptide mixtures (50 mM) by incubation for 2 hours at 30ºC in 1536-well plates in 50 mM HEPES, pH 7.4, 15 mM $MgCl_2$, 0.1 mM Na_3VO_4, 1 mM EGTA, 0.1% BSA, 0.1% Tween 20, and 50 mM γ-^{33}P-ATP (0.03 mCi/ml), essentially as previously described (Chen and Turk, 2010). Aliquots (200 nl) of each reaction were transferred to a streptavidin-coated membrane (Promega), which was processed as described previously (Hutti et al., 2004) and then exposed to a phosphor screen to quantify radiolabel incorporation. For ULKtide phosphorylation assays, the indicated peptide (15 mM) was incubated with ULK1/FIP200/Atg13 complexes in 20 mM HEPES, pH 7.4, 10 mM $MgCl_2$, 1 mM DTT, 0.1% BSA for 15 minutes. At 5 minute intervals, an aliquot of the reaction was spotted onto P81 phosphocellulose filters, which were washed, dried, and subjected to scintillation counting. Assays were performed in duplicate and data show the average of three separate experiments.

Lenti- and retroviral preparation and viral infection

Lentiviral shRNA transduction and retroviral gene expression was performed as described previously (Egan et al., 2011). Briefly, the pQCXIN Myc-Vps34 construct was transfected along with the ampho packaging plasmid into growing HEK-293T cells. Virus-containing supernatants were collected 48 hours after transfection, filtered to eliminate cells, and transferred to target Vps34$^{flox/flox}$ MEFs which were infected in the presence of polybrene. 24 hours later, cells were selected with neomycin.

ULK1 kinase assays

γ-^{32}P-ATP assays to measure ULK1 kinase activity were performed as previously described (Jung et al., 2009). Briefly, Flag-ULK1 was transfected into HEK-293T cells and 20 hours later treated as indicated. The immmunoprecipitate was washed in IP buffer 3 times, and washed in kinase buffer (25 mM MOPS, pH 7.5, 1 mM EGTA, 0.1 mM Na_3VO_4, 15 mM $MgCl_2$,). Hot and cold ATP were added at a 100 μM final concentration. As substrates, GST or the recombinant protein GST-Atg101 purified from *E. coli* were used at 1 μg for each reaction. Reactions were boiled and run out on SDS-PAGE gels. Gels were dried and imaged using PhosphoImager software.

Kinase inhibitor selectivity profiling

Kinase inhibitor specificity profiling assays were first carried out using DiscoveRx KINOMEscan competition binding assay against a panel of 456 kinases (www.discoverx.com) using 1 mM SBI-0206965. Kinases that potentially interacted with SBI-0206965 (inhibited to less than 10% DMSO control) were then tested in classic *in vitro* kinase assays (Reaction Biology; http://www.reactionbiology.com/) with a dose curve of SBI-0206965 to monitor enzymatic activity and determine IC_{50} curves.

Mass spectrometry

Myc-tagged candidate ULK1 substrates were overexpressed in HEK-293T cells as described and immunoprecipitated with anti-Myc antibody, run out on SDS-PAGE gels, and coomassie stained. Bands on the gels corresponding to each candidate were cut out and subjected to reduction with dithiothreitol, alkylation with iodoacetamide, and in-gel digestion with trypsin or chymotrypsin overnight at pH 8.3, followed by reversed-phase microcapillary/tandem mass spectrometry (LC/MS/MS). LC/MS/MS was performed using an Easy-nLC nanoflow HPLC (Proxeon Biosciences) with a self-packed 75 μm id x 15 cm C_{18} column coupled to a LTQ-Orbitrap XL mass spectrometer (Thermo Scientific) in the data-dependent acquisition and positive ion mode at 300 nL/min. Peptide ions from predicted phosphorylation sites were also targeted in MS/MS mode for quantitative analyses. MS/MS spectra collected via collision induced dissociation in the ion trap were searched against the concatenated target and decoy (reversed) single entry and full Swiss-Prot protein databases using Sequest (Proteomics Browser Software, Thermo Scientific) with differential modifications for Ser/Thr/Tyr phosphorylation (+79.97) and the sample processing artifacts Met oxidation (+15.99), deamidation of Asn and Gln (+0.984) and Cys alkylation (+57.02). Phosphorylated and unphosphorylated peptide sequences were identified if they initially passed the following Sequest scoring thresholds against the target database: 1+ ions, Xcorr ≥ 2.0 Sf ≥ 0.4, P ≥ 5; 2+ ions, Xcorr ≥ 2.0, Sf ≥ 0.4, P ≥ 5; 3+ ions, Xcorr ≥ 2.60, Sf ≥ 0.4, P ≥ 5 against the target protein database. Passing MS/MS spectra were manually inspected to be sure that all **b-** and **y-** fragment ions aligned with the assigned sequence and modification sites. Determination of the exact sites of phosphorylation was aided using FuzzyIons and GraphMod and phosphorylation site maps were created using ProteinReport software (Proteomics Browser Software suite, Thermo Scientific). False discovery rates (FDR) of peptide hits (phosphorylated and unphosphorylated) were estimated below 1.5% based on reversed database hits.

Apoptosis analysis - Western blot and flow cytometry

A549 cells (ATCC #CCL185) and wild-type mouse embryonic fibroblasts (MEF) were seeded at a concentration of 2.5 x 10^5 cells/mL (ie. 750,000 cells per 6 cm dish), grown overnight (18 hours), and treated as indicted in the figure legends. Unless otherwise indicated, "starvation" is EBSS and "control" is DMEM with full serum for indicated time points. Samples for Western blot analysis were washed once in 1X ice cold PBS and lysed in boiling SDS lysis buffer (10 mM Tris pH 7.5, 100 mM NaCl, 1% SDS). After trituration, lysates were equilibrated for protein levels using the BCA method (Pierce), resolved on 8 to 15% SDS-PAGE gels depending on the size of the protein, and transferred to PVDF membranes. Membranes were probed with the indicated antibodies overnight according to the manufacturers' instructions.

For flow cytometric analysis, cells were collected at the indicated time point, washed once in PBS, trypsinized, and pelleted. For AnnexinV staining, cells were washed in 1X AnnexinV buffer and stained with AnnexinV and 7-AAD according to the manufacturer's protocol (BD Pharmingen, San Diego, CA). Briefly, cells were re-suspended in AnnexinV buffer to a concentration of 1x10^6/mL. 100,000 cells were then stained with 5 μL of phycoerythrin (PE)-conjugated AnnexinV antibody (BD Pharmingen, San Diego, CA) and 5 μL of 7-amino-actinomycin D (7AAD) and then incubated at room temperature for 15 minutes. 400 μL of AnnexinV buffer was then added to each sample with gentle mixing. Stained cells were analyzed using a FACScan flow cytometer (Becton Dickinson, San Jose, CA). Flow cytometry data was analyzed using FlowJo 8.6 software (Tree Star Inc., Ashland, OR).

Fluorescence microscopy

Vps34$^{flox/flox}$ MEFs were reconstituted with Flag-Vps34 and either p40FX or GFP-DFCP1. 48 hours post-infection with adenovirus expressing Cre recombinase (MOI of 100), cells were plated on glass coverslips at a density of 3x10^5 cells per well in 6-well tissue culture plates. 18 hours later, cells were fixed in 4% PFA in PBS for 10 minutes and permeabilized in 0.2% Triton in PBS for 10 minutes. The following primary antibodies were used: mouse anti-Myc epitope and LC3B XP antibody (#2276 and #3868 respectively, Cell Signaling Technologies). Secondary antibodies used were anti-rabbit Alexa488 and anti-mouse Alexa594 (1:1000; Molecular Probes). Cells were then fixed and counter stained with DAPI. Coverslips were mounted in FluoromountG (SouthernBiothech). Images were acquired on a Zeiss Axioplan2 epifluorescence microscope coupled to the Openlab software. 10 random fields per condition were acquired using the 100X objective and representative images are shown.

General chemical synthesis

All reactions were performed in oven-dried glassware under an atmosphere of nitrogen with magnetic stirring. All solvents and chemicals used were purchased from Sigma-Aldrich or Acros, and were used as received without further purification. Purity and characterization of compounds were established by a combination of liquid chromatography-mass spectroscopy (LC-MS) and NMR analytical techniques and was >95% for all tested compounds. Silica gel column chromatography was carried out using pre-packed silica cartridges from RediSep (ISCO Ltd.) and eluted using an Isco Companion system. ^{1}H- and ^{13}C-NMR spectra were obtained on a Joel 400 spectrometer at 400 MHz and 100 MHz, respectively. Chemical shifts are reported in δ (ppm) relative to residual solvent peaks or TMS as internal standards. Coupling constants are reported in Hz. HPLC-MS analyses were performed on a Shimadzu 2010EV LCMS using the following conditions: Kromisil C18 column (reverse phase, 4.6 mm _ 50 mm); a linear gradient from 10% acetonitrile and 90% water to 95% acetonitrile and 5% water over 4.5 min; flow rate of 1 mL/min; UV photodiode array detection from 200 to 300 nm.

General scheme for the synthesis of 2-(5-bromo-2-(3,4,5-trimethoxyphenylamino)pyrimidin-4-yloxy)-*N*-methylbenzamide (SBI-0206965) (Scheme S1)

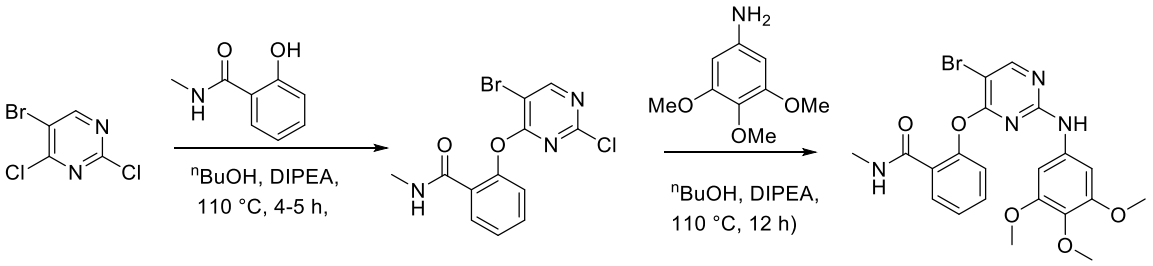

Scheme S1

General Procedure for the synthesis 2-(5-bromo-2-(3,4,5-trimethoxyphenylamino)pyrimidin-4-yloxy)-*N*-methylbenzamide (SBI-0206965)

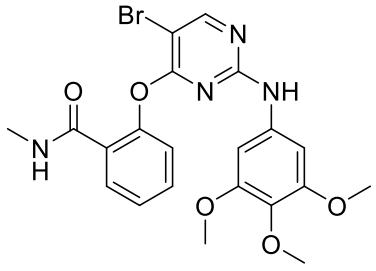

To a solution of 2-hydroxy-N-methylbenzamide (0.151 g, 1 mmol) in ^{n}BuOH (5 mL), were added 5-bromo-2,4-dichloropyrimidine (0.227 g, 1 mmol), and diisopropylethylamine (0.18 mL, 1 mmol). The

reaction mixture was stirred at 110 °C for 4-5 h. It was then cooled to room temperature and to the same reaction mixture was added the 3,4,5-trimethoxyaniline (0.183 g, 1 mmol) and DIPEA (0.17 mL, 1 mmol), and heated at 110 °C for 12 h. The reaction mixture was cooled to room temperature and excess solvent was removed under reduced pressure. The crude residue was purified using automated prep-HPLC to afford the desired compound as a brown solid (0.100 g, 20%). **^{1}H NMR** (DMSO-d_6): δ 9.41 (s, 1H), 8.47 (s, 1H), 8.50-8.03 (m, 1H), 7.56 (dd, J = 7.8 Hz, 1.8 Hz, 1H), 7.50 (t, J = 7.8 Hz, 1H), 7.32-7.29 (m, 2H), 6.80 (s, 2H), 3.62 (s, 9H), 2.60 (d, J = 4.5 Hz, 3H). **^{13}C NMR** (DMSO-d_6): δ 166.1,164.9, 160.5, 158.7, 153.1, 150.0, 136.6, 131.4, 130.7, 130.0, 129.5, 126.3, 123.7, 97.5, 60.5, 56.2, 26.6. LC-MS (ESI) calcd. for $C_{21}H_{21}BrN_4O_5$ $[M+H]^+$: 491.07; found: 491.0. HRMS (ESI) calcd. for $C_{21}H_{21}BrN_4O_5$ $[M+H]^+$: 491.0751; found: 491.0761.

References

Chen, C., and Turk, B.E. (2010). Analysis of serine-threonine kinase specificity using arrayed positional scanning peptide libraries. Curr Protoc Mol Biol *Chapter 18*, Unit 18 14.

Egan, D.F., Shackelford, D.B., Mihaylova, M.M., Gelino, S., Kohnz, R.A., Mair, W., Vasquez, D.S., Joshi, A., Gwinn, D.M., Taylor, R.*, et al.* (2011). Phosphorylation of ULK1 (hATG1) by AMP-activated protein kinase connects energy sensing to mitophagy. Science *331*, 456-461.

Hutti, J.E., Jarrell, E.T., Chang, J.D., Abbott, D.W., Storz, P., Toker, A., Cantley, L.C., and Turk, B.E. (2004). A rapid method for determining protein kinase phosphorylation specificity. Nat Methods *1*, 27-29.

Jung, C.H., Jun, C.B., Ro, S.H., Kim, Y.M., Otto, N.M., Cao, J., Kundu, M., and Kim, D.H. (2009). ULK-Atg13-FIP200 complexes mediate mTOR signaling to the autophagy machinery. Mol Biol Cell *20*, 1992-2003.

Personnel Receiving Pay from the Research Effort:

Fund Year:	Name	Title
04/01/2013 – 03/31/2014	Laurie Gerken	Research Assistant II
	Debbie Ross	Research Assistant II
04/01/2014 – 03/31/2015	Laurie Gerken	Research Assistant II
	Debbie Ross	Research Assistant II
04/01/2015 – 03/31/2016	Laurie Gerken	Research Assistant II
	Debbie Ross	Research Assistant II
	Liliana Vera	Research Assistant II